J. Fluid Mech. (2001), *vol.* 427, *pp.* 241–274. Printed in the United Kingdom

Lagrangian characteristics of turbulence and scalar transport in direct numerical simulations

By P. K. YEUNG

School of Aerospace Engineering, Georgia Institute of Technology, Atlanta, GA 30332, USA
e-mail: yeung@peach.ae.gatech.edu

(Received 8 September 1999 and in revised form 25 July 2000)

A study of the Lagrangian statistical properties of velocity and passive scalar fields using direct numerical simulations is presented, for the case of stationary isotropic turbulence with uniform mean scalar gradients. Data at higher grid resolutions (up to 512^3 and Taylor-scale Reynolds number 234) allow an update of previous velocity results at lower Reynolds number, including intermittency and dimensionality effects on vorticity time scales. The emphasis is on Lagrangian scalar time series which are new to the literature and important for stochastic mixing models. The variance of the 'total' Lagrangian scalar value ($\tilde{\phi}^+$, combining contributions from both mean and fluctuations) grows with time, with the velocity–scalar cross-correlation function and fluid particle displacements playing major roles. The Lagrangian increment of $\tilde{\phi}^+$ conditioned upon velocity and scalar fluctuations is well represented by a linear regression model whose parameters depend on both Reynolds number and Schmidt number. The Lagrangian scalar fluctuation is non-Markovian and has a longer time scale than the velocity, which is due to the strong role of advective transport, and is in contrast to results in an Eulerian frame where the scalars have shorter time scales. The scalar dissipation is highly intermittent and becomes de-correlated in time more rapidly than the energy dissipation. Differential diffusion for scalars with Schmidt numbers between 1/8 and 1 is characterized by asymmetry in the two-scalar cross-correlation function, a shorter time scale for the difference between two scalars, as well as a systematic decrease in the Lagrangian coherency spectrum up to at least the Kolmogorov frequency. These observations are consistent with recent work suggesting that differential diffusion remains important in the small scales at high Reynolds number.

1. Introduction

It is well-known (e.g. Monin & Yaglom 1971) that in many problems of turbulent mixing and dispersion the dominant mechanism is advective transport, whereby the material or flow property being 'mixed' is carried along with the disorderly motion described by the velocity fluctuations. In these situations it is particularly useful to adopt a Lagrangian viewpoint, with an observer following the motion of a collection of fluid particles that together constitute the fluid continuum. The description of turbulent transport in terms of fluid particle displacement and velocity in fact dates back to the work of G. I. Taylor (1921). The close connection between turbulent dispersion and fluid particle motion is also the underlying principle behind the well-

established use of Lagrangian approaches in the modelling of pollutant transport in the environment (e.g. Csanady 1973; Sawford 1985; Thomson 1996).

In this paper we consider the Lagrangian description of turbulence, with special emphasis on the transport of passive scalars subject to molecular mixing. Apart from fundamental understanding we also aim at providing information useful for modelling. In particular we note that in the probability density function (PDF) approach (reviewed by Pope 1985 and Dopazo 1994) for calculating turbulent flows, although nonlinear convective and reaction terms are in closed form, molecular effects must still be modelled. Because of high dimensionality, for computational efficiency it is usual to solve modelled PDF equations using Monte-Carlo formulations, where the fluid medium is effectively replaced by a set of discrete fluid particles in a Lagrangian frame. Consequently, there is considerable interest in the behaviour of the Lagrangian time series of scalar fluctuations following fluid particle trajectories. This type of information is in fact crucial for stochastic models of turbulent mixing, such as binomial models proposed by Valiño & Dopazo (1990, 1991) and the more recent Lagrangian spectral relaxation (LSR) model of Fox (1997, 1999).

Lagrangian statistics are a prime example of turbulence quantities which are extremely difficult to measure in experiments but readily accessible by direct numerical simulations (DNS). Indeed, despite some recent progress (Voth, Satyanarayanan & Bodenschatz 1998), because of the need to follow the paths of 'tagged' fluid particles over time, Lagrangian measurements in the laboratory are still difficult and subject to considerable uncertainty. On the other hand, in DNS since instantaneous velocity fields in three-dimensional space are available it is relatively straightforward (first demonstrated by Riley & Patterson 1974) to calculate fluid particle velocities by interpolation and hence to follow particle trajectories. Lagrangian quantities from DNS reported in the literature include, for example, velocity autocorrelations and structure functions in isotropic turbulence (Yeung & Pope 1989), anisotropy and non-stationarity effects in homogeneous shear flow (Squires & Eaton 1991), particle-pair dispersion in stratified turbulence (Kimura & Herring 1996), and the statistics of fluid particle acceleration (Yeung 1997). Lagrangian data from DNS have also been used for the modelling of fluid particle motion using stochastic and kinematic approaches (e.g. Sawford 1991; Heppe 1998; Malik & Vassilicos 1999).

As noted by Pope (1994) the stochastic modelling of scalars is both more challenging and less developed than that for the velocity. At the same time, although Lagrangian scalar statistics along fluid particle trajectories can be obtained from DNS, apart from some very recent calculations (Brethouwer 2000) this type of data is still virtually unknown in the literature. Our primary objective is thus to provide a basic characterization of Lagrangian scalar statistics in a simplified configuration, namely for homogeneous passive scalar fields with uniform mean gradients in stationary isotropic turbulence. This scenario incorporates the physics of both production and dissipative mechanisms which together produce statistical stationarity in time for the scalar fluctuations. We also study Lagrangian aspects of differential diffusion between multiple scalars with different molecular diffusivities, which is especially important (Bilger & Dibble 1982) in problems of non-premixed combustion. As a process of molecular origin, differential diffusion is often thought to be less important at higher Reynolds number (e.g. Nilsen & Kosály 1997). However recent studies using high-resolution DNS (Yeung 1996, 1998) show that diffusivity effects remain important in the small scales, whereas in experiments (Saylor & Sreenivasan 1998) they are found to be significant also at scales larger than the Batchelor scale. The modelling of multi-scalar mixing often involves additional challenges (e.g. Ulitsky & Collins 2000).

Lagrangian data are expected to provide useful complementary time-scale information for stochastic models of differential diffusion (e.g. Tsai & Fox 1995; Fox 1999).

In the present study we extract Lagrangian information from direct numerical simulations using up to 512^3 grid points with a Taylor-scale Reynolds number (averaged over time) approximately 230 – which (as shown in Yeung & Zhou 1997) is sufficiently high to exhibit classical inertial-range properties in the Eulerian energy spectrum in a manner consistent with experiments. The current availability of high-resolution DNS data also provides an opportunity for an update of Lagrangian velocity statistics previously reported at lower Reynolds number (Yeung & Pope 1989). To address the dependence of scalar statistics on Reynolds and Schmidt numbers we have performed simulations at four grid resolutions from 64^3 to 512^3, with Schmidt numbers in the range $1/8$ to 1. In addition to velocity components and scalar fluctuations we have also obtained the Lagrangian time series of small-scale variables such as velocity gradients and scalar gradients (and hence the corresponding dissipation rates). The Lagrangian evolution of the velocity gradient tensor is relevant to studies of turbulent flow structure (Ooi *et al.* 1999). Furthermore, for turbulent mixing the scalar dissipation and its Lagrangian time scale are important in both the LSR model of Fox (1997) and in the modelling of conditional variance (Swaminathan & Bilger 1999) using the conditional moment closure approach (Klimenko & Bilger 1999).

The remaining sections of this paper are organized as follows. In § 2 we give a brief description of the numerical approach employed and of the statistical sampling issues specific to Lagrangian quantities. In § 3 we provide a brief overview of the qualitative properties of typical time series extracted from DNS. Quantitative results are given in § 4, with separate subsections devoted to statistics of the velocity, those of passive scalars taken first individually, and then in pairs of scalars of different molecular diffusivities. Quantities reported include auto- and cross-correlation functions, integral time scales, and spectra in frequency space. Finally in § 5 we summarize the present results and briefly discuss their future use for modelling.

2. Numerical approach

As in previous work (Yeung 1996, 1998) we perform direct numerical simulations of instantaneous, three-dimensional momentum and passive scalar transport equations using a parallel version of the algorithm of Rogallo (1981). The numerical method is Fourier pseudo-spectral in space and second-order Runge–Kutta in time. Velocity fluctuations in isotropic turbulence are made statistically stationary by numerical forcing at the large scales using the scheme of Eswaran & Pope (1988*a*). Grid resolutions and Taylor-scale Reynolds numbers (R_λ) are as given in table 1 which also contains other relevant parameters discussed later in this Section. Both the numerical simulations and subsequent data analysis were performed on an IBM SP supercomputer using up to 64 parallel processors in the case of a 512^3 grid.

To obtain Lagrangian information we use the particle-tracking algorithm of Yeung & Pope (1988). A fourth-order-accurate and twice-differentiable cubic spline interpolation scheme is used to calculate the fluid particle velocity ($\boldsymbol{u}^+$) from the Eulerian velocity field, based on the relation

$$\boldsymbol{u}^+(t) = \boldsymbol{u}(\boldsymbol{x}^+[t], t) \tag{1}$$

where the superscript $^+$ denotes Lagrangian quantities and $\boldsymbol{x}^+$ is the instantaneous particle position vector. The same interpolation scheme can be used to calculate

Grid	64^3	128^3	256^3	512^3
R_λ	38	91	134	234
Sc	1/4, 1/2, 1	1/8, 1/2, 1	1/8, 1	1/8, 1
$k_{max}\eta$	1.46	1.41	1.41	1.40
h/τ_η	0.25	0.25	0.18	0.20
T/T_E	13.6	11.7	10.4	8.0
M	16 384	16 384	32 768	106 496

TABLE 1. Major parameters of the numerical simulations.

Lagrangian values of the turbulent fluctuations of other quantities, including passive scalars, velocity gradients and scalar gradients at the instantaneous particle position. Since these quantities are not involved in the determination of fluid particle trajectories the additional interpolations are not required at every time step but only at regular output time intervals. There is thus only a small increase in CPU requirements.

As in Yeung (1998) we consider exclusively scalar fluctuations evolving under the action of a uniform gradient in the mean scalar field (Φ), as

$$\frac{\partial \phi}{\partial t} + u_i \frac{\partial \phi}{\partial x_i} = -u_i \frac{\partial \Phi}{\partial x_i} + D_\phi \frac{\partial^2 \phi}{\partial x_i \partial x_i}, \tag{2}$$

where the molecular diffusivity D_ϕ may be different for each scalar. It is important to note that the scalar value following a fluid particle consists of contributions from both the mean and fluctuating scalar fields sampled at the instantaneous particle position. For the choice $\nabla\Phi = (G, 0, 0)$ we can formally write

$$\tilde{\phi}^+(t) = Gx^+(t) + \phi^+(t) \tag{3}$$

where $\tilde{\phi}^+(t)$ is henceforth referred to as the Lagrangian *total* scalar value, and $\phi^+(t) = \phi(\boldsymbol{x}^+[t], t)$ is the Lagrangian *fluctuation* relative to the local value of the mean profile $\Phi = Gx$. In other words, the Lagrangian value of the scalar carries two sources of randomness: one due to the motion of the fluid particle up (or down) the mean scalar gradient, and the other due to the scalar fluctuation as a function of spatial location. We study the properties of both $\tilde{\phi}^+$ and ϕ^+.

Attainment of stationarity in time for both velocity and scalars allows standard techniques of time series analysis to be applied. Time-scale information is expressed by the autocorrelation function which for any stationary variable X of mean μ_X and variance $\mathrm{Var}(X)$ is given by an even function of the time lag (τ) alone, in the form

$$\rho_X(\tau) = \frac{\langle (X(t) - \mu_X)(X(t+\tau) - \mu_X) \rangle}{\mathrm{Var}(X)}, \tag{4}$$

with the corresponding integral time scale defined by

$$\mathscr{T}_X = \int_0^\infty \rho_X(\tau)\, \mathrm{d}\tau. \tag{5}$$

It should be noted that the estimation of the autocorrelation function from finite-time records (of length T) is not a trivial matter (see Priestley 1981, § 5.3 for details), and standard versions of unbiased and biased estimators can be distinguished. (A finite-sample estimate of a statistical quantity is said to be biased if its expected value is not equal to the true, or theoretical, mean value.) The unbiased and biased estimators in this case differ by a normalization factor which determines the treatment of sampling

noise at large time lags for which relatively few samples are available. As described in Yeung & Pope (1988, Appendix A; 1989, § 3) we use both unbiased and biased versions, and for different purposes. Specifically, we use the unbiased estimator for $\rho_X(\tau)$ to estimate the integral time scale, while here also truncating the last 10% of the range of time lag that is most prone to contamination by sampling noise. On the other hand, because only the biased estimate of $\rho_X(\tau)$ is positive definite, it is used to obtain the Lagrangian frequency spectrum (which must be positive) via a Fourier cosine transform.

Whereas the autocorrelation measures the correlation coefficient between the same variable at times t and $t+\tau$, there is also interest in the correlation between different variables at different times. Examples include the cross-correlation between a scalar and the velocity component in the direction of its mean gradient, and between each scalar and its dissipation rate (Fox 1997). For two random variables X and Y the *cross*-correlation function is defined by

$$\rho_{XY}(\tau) = \frac{\langle (X(t)-\mu_X)(Y(t+\tau)-\mu_Y)\rangle}{[\mathrm{Var}(X)\mathrm{Var}(Y)]^{1/2}}. \tag{6}$$

Unlike the autocorrelation, the cross-correlation is in general not an even function of τ. In fact, its deviation from evenness (or symmetry) can sometimes be taken as an indicator of cause-and-effect relationships: for example if $\rho_{XY}(\tau)$ is stronger for positive τ versus negative τ then it suggests the 'current' value of X at time t may have a strong influence on the value of Y in the 'near' future specified by a modest range of $\tau > 0$. We also note that $\rho_{XY}(0)$ is the same as $\rho(X,Y)$, the correlation coefficient between X and Y.

The accuracy of Lagrangian statistics from DNS depends on several factors. First, it is clear that the Eulerian DNS calculation itself must be well-resolved in space, and that an accurate interpolation scheme (in this case cubic splines) be employed. Spatial resolution is measured by the parameter $k_{max}\eta$ where k_{max} is the highest wavenumber resolved by the grid and η is the Kolmogorov length scale. A value of about 1.5 is considered adequate for the velocity and helps ensure accurate particle trajectories although it may still be limiting for scalars of $Sc \geqslant 1$ exhibiting more small-scale spectral content than the velocity fluctuations. Second, Lagrangian data must be sampled at time intervals (h) sufficiently small compared to the Kolmogorov time scale (τ_η) so that high-frequency changes can be captured. Because some variables (such as small-scale quantities) following a fluid particle may change more rapidly than others, the high-frequency parts of Lagrangian spectra must be interpreted with caution. Third, the simulation data must span a period (T) large compared to the large-eddy turnover time (T_E, defined as ratio of longitudinal integral length scale to the r.m.s. velocity) of the turbulence, so that stable time averages with a good degree of isotropy can be obtained. This requirement is made more stringent by the fact that (see Appendix of Yeung & Pope 1989) the method of forcing used in this work tends to introduce large variations of Eulerian statistics in time. Finally there needs to be a sufficiently large ensemble of particles (M) being tracked for averaging. It should be noted that (Tennekes & Lumley 1972) in homogeneous turbulence Eulerian 'one-point' averages taken over all the grid points are formally equivalent to Lagrangian 'one-particle' averages taken over a collection of individual fluid particles at a given time. In practice, by specifying a tolerance on this criterion and computing statistical confidence intervals we find that the number of particle samples needed increases with Reynolds number, which is consistent with the fact that a wider range of scales is being simulated.

Table 1 shows actual values of the parameters $k_{max}\eta$, h/τ_η, T/T_E and M in the simulations. Although the degree of accuracy achieved varies with the quantity considered, the parameter choices listed here have allowed us to satisfy the major requirements above in an overall manner, to the extent allowed by the CPU resources available.

3. Typical time series

Prior to quantitative analyses it is useful to have a qualitative view of the Lagrangian time series by looking at some typical sample traces, of the type appearing in work by other authors (Pope 1994, 2000; Fox 1997) but here obtained from DNS. For this purpose it is neither necessary nor possible to consider every fluid particle tracked but we find that a small sample of several for each flow variable is sufficient. Accordingly in figure 1 we show eight sample time traces (lines A to H) from the 512^3 simulation for several variables following Lagrangian particle trajectories, namely: (*a*) a velocity component, (*b*) energy dissipation rate ($\epsilon \equiv 2\nu s_{ij}s_{ij}$, where s_{ij} is the fluctuating strain rate), (*c*) scalar with $Sc = 1/8$, (*d*) scalar with $Sc = 1$, (*e*) difference between the scalars, and (f, g) the corresponding dissipation rates for each scalar ($\chi \equiv 2D_\phi(\partial\phi/\partial x_i)^2$). Each of the traces shown span a time period of nearly 11 Lagrangian integral time scales (T_L) of the velocity. All of the data shown are normalized: by either an r.m.s. value (σ, with σ_u being averaged over three velocity components), or, in the case of non-negative quantities (ϵ and χ), by their global mean value. Comments on each sub-figure are given below. (Because of its somewhat compressed nature, this plot needs to be read carefully.)

To begin, the velocity in (*a*) is shown mainly for reference purposes. As expected its time trace is smooth and without abrupt changes. The velocity PDF is close to Gaussian, with near zero skewness and flatness factor in the range 2.8–3.0. In (*b*) we see that the energy dissipation changes more quickly in time than the velocity, with intense but short-lived bursts of activity (line H, at $t/T_L \approx 1.6$) at levels much higher than the mean. These characteristics suggest a behaviour in the Lagrangian frame that is consistent with established notions of intermittency (e.g. Frisch 1995, p. 122). In particular, besides their intensity the short-lived nature of the intermittent bursts is an essential feature, since if these 'bursts' were long-lasting then the 'large' dissipation samples they contain would no longer be rare, and in fact would not be so large anymore when normalized by an increased global mean value. (Incidentally, the infrequent occurrence of these bursts illustrates the importance of having several traces in the figure, in order to ensure a representative sample over time.) Since the time series are recorded along the fluid particle trajectory these observations also imply that the typical residence time of a fluid particle in a region of intense dissipation is short. In turn this is consistent with the known spottiness of dissipation fluctuations and other small-scale parameters in space (Sreenivasan & Antonia 1997).

In (*c*) and (*d*) it can be seen that, in comparison to the velocity in (*a*), the Lagrangian scalar fluctuations are relatively slowly changing. It should be noted that, according to (2) in the hypothetical case of a non-diffusive scalar ($D_\phi = 0, Sc = \infty$) the Lagrangian rate of change of the scalar fluctuation would be proportional (via the mean gradient term) to the velocity. If this statement is in practice a good approximation then it implies that the scalar evolves like a time integral of the velocity and thus changes more slowly than the velocity itself. Corresponding time traces (matching the lettered symbols) of the two scalars are seen to be very close to each other, suggesting that

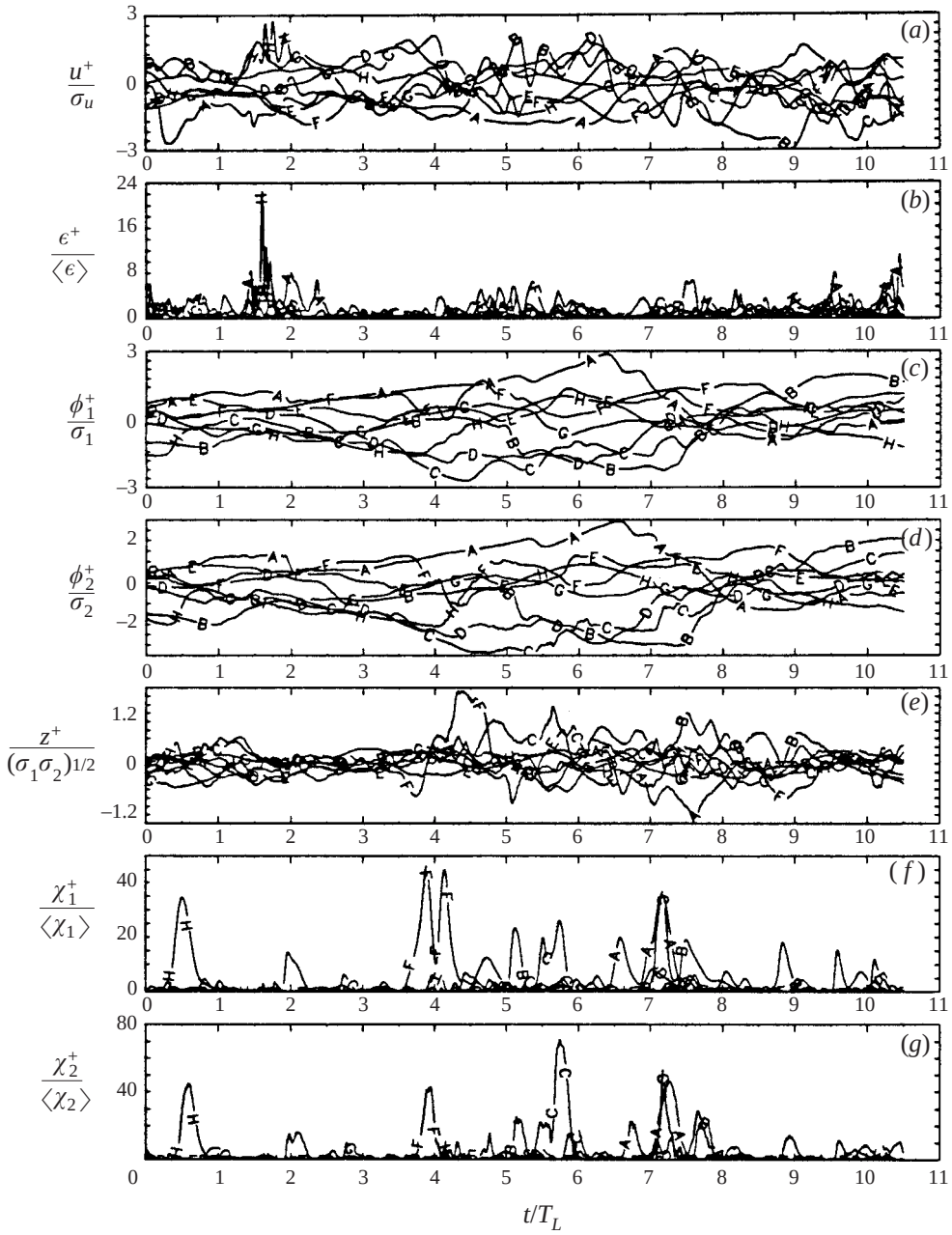

FIGURE 1. Typical Lagrangian time series of normalized Lagrangian quantities from the 512^3 simulation: (*a*) velocity, (*b*) energy dissipation, (*c*) scalar ϕ_1 with $Sc = 1/8$, (*d*) scalar ϕ_2 with $Sc = 1$, (*e*) difference $z = \phi_1 - \phi_2$, (*f*) dissipation of ϕ_1, and (*g*) dissipation of ϕ_2. Each data line (A to H) represents a different fluid particle in the sample.

molecular diffusion has only a small effect on the time history of a scalar value following the particle trajectories.

Despite the apparent closeness between scalars with $Sc = 1/8$ and $Sc = 1$ noted above, in (*e*) we find a considerable contrast for the difference z between them. Indeed,

although (due to the scalars being highly correlated with each other) the difference is of smaller magnitude, it is characterized by much more rapid changes in time. This suggests that molecular diffusivity effects for two-scalar statistics are stronger at small time scales or equivalently at high-frequencies. Furthermore, the occurrence of occasional 'bursts' in the time series of z (e.g. line F at $t/T_L \approx 4.5$) indicates at least a mild degree of intermittency. It would be of interest in the future to explore the possibly complex connections between these bursts and other fluid dynamic variables along the particle trajectories.

In (f) and (g) we observe that, like the energy dissipation, the scalar dissipation time series are also characterized by intermittency. In fact, with the scales on the ordinate showing samples reaching higher normalized peak intensities, the data suggest that, especially for $Sc = 1$ but even for $Sc = 1/8$, the scalar dissipation is more intermittent than the energy dissipation. This observation of intermittency is consistent with Eulerian results in Overholt & Pope (1996) and is also supported by calculations of skewness and flatness factors. In addition it may be seen that *some* of the intermittent bursts (e.g. line H at $t/T_L \approx 0.5$) in different scalars appear to occur at about the same time. (Note that, to make this observation, one needs to follow individual letters for different lines in the plot very carefully.) This inherently Lagrangian observation is consistent with previous results (Yeung 1998) showing that the gradients (which contribute to the dissipation) of different scalars are significantly correlated.

To conclude this Section, it is important to emphasize the difference between Eulerian and Lagrangian frames of reference. Comparisons are made in figure 2 with Eulerian time series recorded at fixed locations in space, for the velocity and two scalars in the $R_\lambda = 90$ simulation. It can be seen that, whereas in a Lagrangian frame the scalar changes more slowly than the velocity, in an Eulerian frame the opposite is true. The effects of Schmidt number on the two types of time series are also qualitatively different, in that an increase in Sc causes the scalar fluctuation to change (slightly) more slowly in a Lagrangian frame, but (significantly) more quickly in an Eulerian frame. It should be noted that in other studies the passive scalar field at $Sc = 1$ is known to have a greater degree of small-scale content in its spectrum compared to the velocity (Overholt & Pope 1996; Yeung 1998). Usually one expects this property to lead to more rapid changes in time for the scalar fluctuations, but the results here show that this expectation holds only in an Eulerian frame. Since Eulerian and Lagrangian rates of change are given respectively by the unsteady time derivative ($\partial/\partial t$) and material derivative (D/Dt), the significant differences observed here indicate a strong role for advective transport which provides the difference between these two derivative operators. These differences are further quantified via Taylor time scales in § 4.2.

4. Quantitative results and discussion

In this Section we present results from analyses of Lagrangian time series of the type shown in figure 1. Our results are organized into three categories, namely Lagrangian statistics of the velocity field, of each scalar taken separately, and finally of pairs of scalars taken jointly in the context of differential diffusion.

4.1. *Velocity, dissipation and enstrophy*

Lagrangian statistics of the velocity field in isotropic turbulence were first reported by Yeung & Pope (1989) based on DNS data in the range $R_\lambda \sim 38$–93. Observations previously made concerning Lagrangian time scales include: (i) the acceleration vector

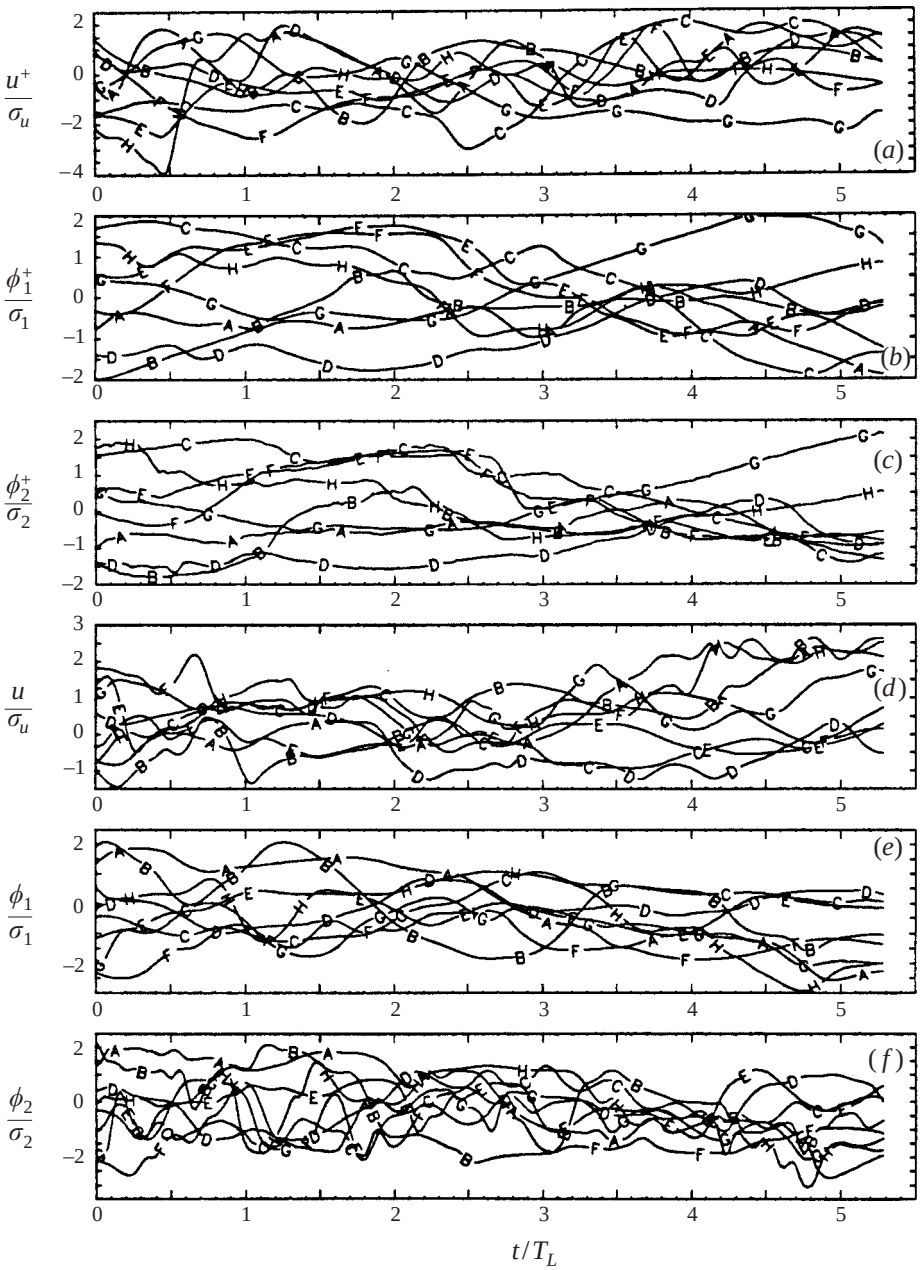

FIGURE 2. Comparison between normalized Lagrangian (*a–c*) and Eulerian time series (*d–f*) for velocity component and scalar fluctuations with $Sc = 1/8$ and $Sc = 1$, taken from the 128^3 simulation.

rotates on a time scale about twice the Kolmogorov time scale but its variance has non-universal behaviour when scaled by Kolmogorov variables, (ii) the ratio of Lagrangian integral time scale to Eulerian eddy-turnover time (T_E) is about 0.72 in this type of flow and insensitive to Reynolds number, and (iii) the integral time scale of enstrophy is longer than that of energy dissipation, but with both appearing to scale with T_L. The present data for the velocity field are obtained and analysed

Grid	64^3	128^3	256^3	512^3
R_λ	38	91	134	234
T_L/τ_η	5.64	9.23	12.6	19.8
T_L/T_E	0.802	0.758	0.795	0.763
$\mathscr{T}_\epsilon/T_L$	0.498	0.401	0.361	0.296
$\mathscr{T}_\epsilon/\tau_\eta$	2.81	3.70	4.55	5.86
$\mathscr{T}_{\partial u/\partial x}/T_L$	0.388	0.215	0.166	0.104
$\mathscr{T}_{\partial u/\partial x}/\tau_\eta$	2.19	1.98	2.09	2.06
$\mathscr{T}_{\partial u/\partial y}/T_L$	0.965	0.688	0.486	0.316
$\mathscr{T}_{\partial u/\partial y}/\tau_\eta$	5.44	6.35	6.12	6.26
$\mathscr{T}_{\omega_x}/T_L$	1.347	0.894	0.691	0.440
$\mathscr{T}_{\omega_x}/\tau_\eta$	7.60	8.25	8.71	8.71
$\mathscr{T}_{\omega_x^2}/T_L$	0.793	0.563	0.429	0.267
$\mathscr{T}_{\omega_x^2}/\tau_\eta$	4.47	5.20	5.41	5.29
$\mathscr{T}_{\omega_x^2+\omega_y^2}/T_L$	0.882	0.635	0.510	0.330
$\mathscr{T}_{\omega_x^2+\omega_y^2}/\tau_\eta$	4.97	5.86	6.43	6.53
$\mathscr{T}_{\omega^2}/T_L$	0.943	0.705	0.562	0.370
$\mathscr{T}_{\omega^2}/\tau_\eta$	5.32	6.51	7.08	7.33
$\mathscr{T}_\epsilon/\mathscr{T}_{\omega^2}$	0.528	0.568	0.642	0.800

TABLE 2. Integral time scales of velocity field parameters.

in a similar manner as in Yeung & Pope (1989). However, the availability of high-resolution data now allows, depending on the quantities being considered, either a stronger confirmation or a clearer re-examination of Reynolds number dependence. Various time-scale ratios are shown in table 2, where $\mathscr{T}$ is used as a generic symbol for integral time scales of quantities other than the velocity.

Observation (i) from Yeung & Pope (1989) as stated above has received support from more recent work involving DNS data at higher resolution (Yeung 1997; Vedula & Yeung 1999) as well as a theoretical model based on coherent structures (Gotoh & Rogallo 1999). Data for the ratio T_L/T_E in table 2 are consistent with (ii), with a nominal value only slightly higher than that previously reported. However, for item (iii) the high-resolution data reveal a different behaviour. Specifically, the integral time scales for both dissipation and (especially) enstrophy are now seen to decrease steadily with respect to T_L at increasing Reynolds number, in such a way that these two time scales ($\mathscr{T}_\epsilon$, $\mathscr{T}_{\omega^2}$) become closer to each other.

The new information in table 2 includes data on velocity gradients, and alternative normalization by τ_η. As one might expect from their small-scale content, single-component velocity gradients such as $\partial u/\partial x$ and $\partial u/\partial y$ appear to scale with τ_η. However, some of these time scales (e.g. $6\tau_\eta$ for $\partial u/\partial y$) are actually closer to T_L than to τ_η. Quantities derived from the sums of squares of multiple components (especially ϵ, and to a lesser extent ω^2) tend to have longer time scales which also have a significant Reynolds number dependence. The reasons for this difference are in part addressed in the paragraphs below.

To further illustrate the differences noted here we show in figure 3(a, b) the auto-correlations of several variables at the lowest and highest Reynolds numbers in the

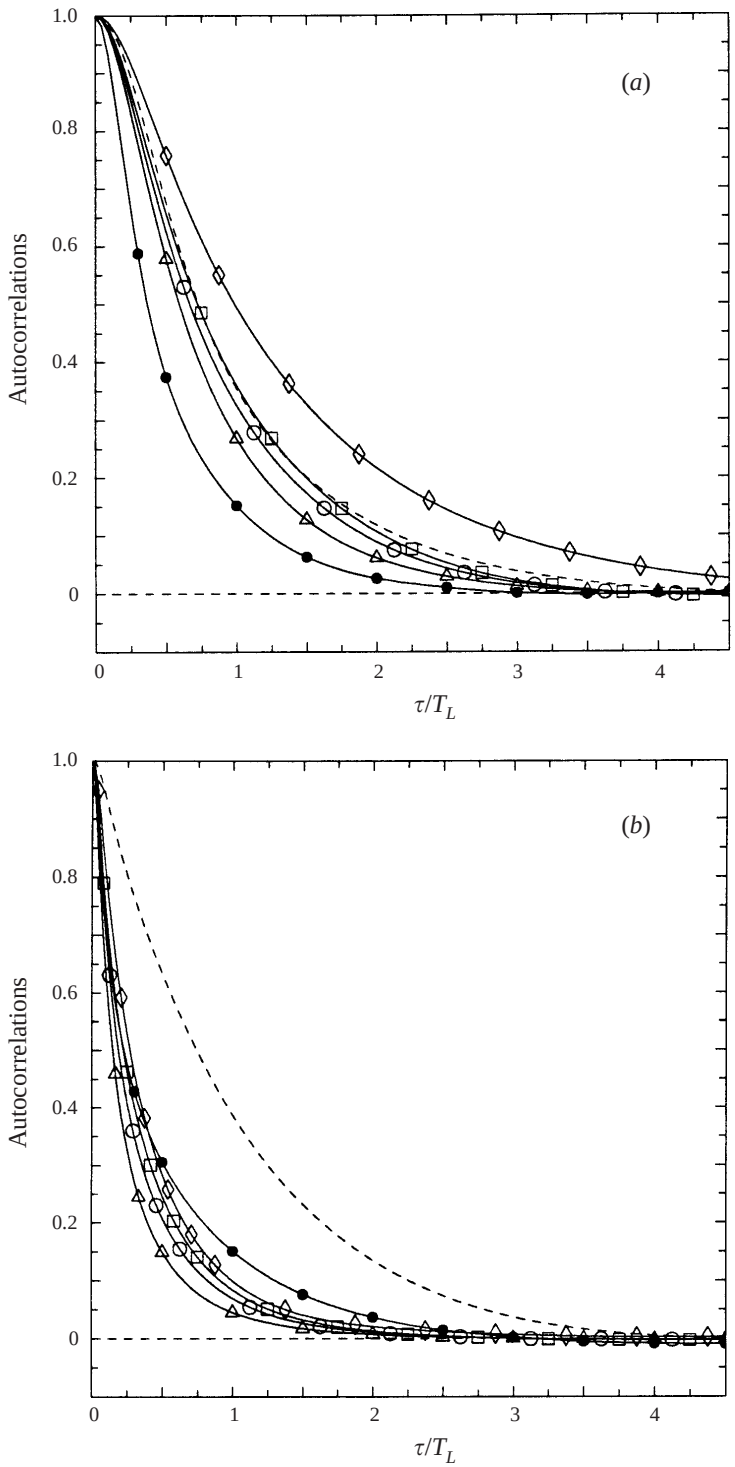

FIGURE 3. Lagrangian autocorrelations of velocity (dashed line), vorticity component (◇), square of one vorticity component (△), sum of squares of two components (○), enstrophy (□), and energy dissipation rate (●). The time lag (τ) is normalized by the Lagrangian integral time scale (of the velocity, T_L). Data taken from (*a*) 64^3 simulation at $R_\lambda = 38$ and (*b*) 512^3 simulation at $R_\lambda = 234$.

simulations. All curves are normalized by the same time scale (T_L) at the given Reynolds number, so that a curve that drops faster would indicate more rapid de-correlation, or a shorter 'memory' time for the variable it represents. Since enstrophy is the sum of squares of three vector components, we investigate here a possible 'componentiality' effect by comparing the autocorrelations of (i) a single vorticity component (of variance σ_ω^2), (ii) its square, (iii) the sum of squares of two components, written as (being statistically equivalent to) $\omega_x^2 + \omega_y^2$, and (iv) the enstrophy itself, considering all three coordinate components. (Although item (ii) here seems a bit contrived it does provide a useful linkage between the statistics of single coordinate components in one dimension and the squares of vector magnitudes in three dimensions.)

Comparison of figures 3(a) and 3(b) indicates that as the Reynolds number increases, all curves except those for the velocity are shifted towards the left, implying more rapid de-correlation relative to the velocity. This effect is most dramatic for the case of a single vorticity component, which, remarkably, has an integral time scale longer than that of the velocity in the 64^3 simulation. At the same time, at all Reynolds numbers we find that the autocorrelations for the vorticity variables follow the ordering implied by the integral time scales in table 2, i.e.

$$\mathscr{T}_{\omega_x^2} < \mathscr{T}_{\omega_x^2+\omega_y^2} < \mathscr{T}_{\omega^2} < \mathscr{T}_{\omega_x}. \tag{7}$$

The ordering here can in part be understood by examining time series samples shown in figure 4. It is well known that vorticity fluctuations are intermittent, which in a Lagrangian frame implies the occurrence of relatively short-lived excursions to large deviations from the mean. Between figures 4(c) and 4(d) it can be seen that this intermittency is stronger when the square of a vorticity component is taken. Because of their high intensity level these intermittent bursts have a strong effect on the autocorrelation; yet since they are infrequent and short-lived the integral time scale is significantly reduced. On the other hand, as the dimensionality is increased from 1 to 3 (figure 4(c, d, e)) large vorticity can now arise from large fluctuations in any or more than one coordinate component. As a result bursts of intense activity become more common (although not as strong when measured by the respective mean values), and together they account for a more significant fraction of the sampling time period. This effect causes ω^2 to remain correlated for longer time intervals than $\omega_x^2 + \omega_y^2$ (and, in turn, ω_x^2), and is indeed reflected in slight increases of time scales in table 2. Furthermore, because of their inherently kinematic nature we expect these arguments to apply also at high Reynolds number.

In figure 4 it can also be seen that the time series of both (especially) enstrophy and dissipation from the 64^3 simulation (parts a, b) are characterized by slower changes measured by T_L when compared with 512^3 data (parts f, g). Since slower changes imply longer memory times this is consistent with the Reynolds number trends for integral time scales given in table 2.

In addition to time-scale information, the frequency content of Lagrangian time series is also important. This is represented by the frequency spectrum which is essentially a Fourier (cosine) transform of the autocorrelation function and is computed using a procedure that attempts to minimize the effects of sampling noise at high frequencies (see Appendix A of Yeung & Pope 1988). At sufficiently high Reynolds numbers classical Kolmogorov scaling arguments suggest an inertial-range form for the Lagrangian velocity frequency spectrum, as

$$E^L(\omega) = B\langle\epsilon\rangle\omega^{-2} \qquad (\pi/T_L \ll \omega \ll \pi/\tau_\eta) \tag{8}$$

where ω is the frequency (which is standard notation and should not be confused

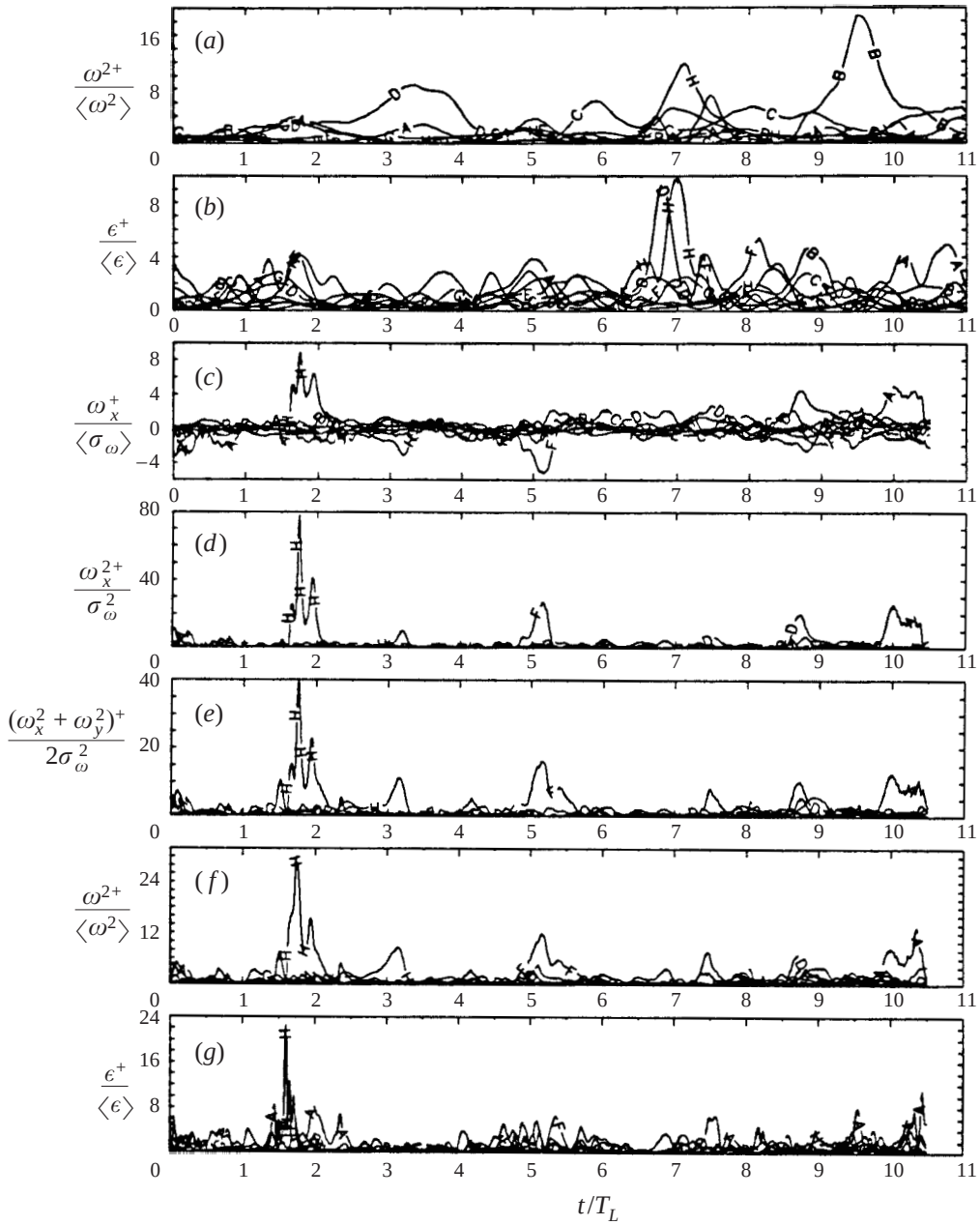

FIGURE 4. Lagrangian time series of normalized vorticity, enstrophy and dissipation: (*a*) enstrophy and (*b*) dissipation from the 64^3 simulation, all others from 512^3: (*c*) vorticity component (*d*) square of vorticity component, (*e*) sum of squares of two vorticity components, (*f*) enstrophy, and (*g*) dissipation.

with similar symbols like ω_x, ω^2 associated with the vorticity), τ_η is Kolmogorov time scale, and B is assumed to be an universal constant. Accordingly data from four grid resolutions are shown in figure 5 in a normalized form to compare with (7). A rough estimate cited in Tennekes & Lumley (1972) is $B \approx C_K^{3/2}$ where C_K is the Kolmogorov constant in the three-dimensional energy spectrum function. With

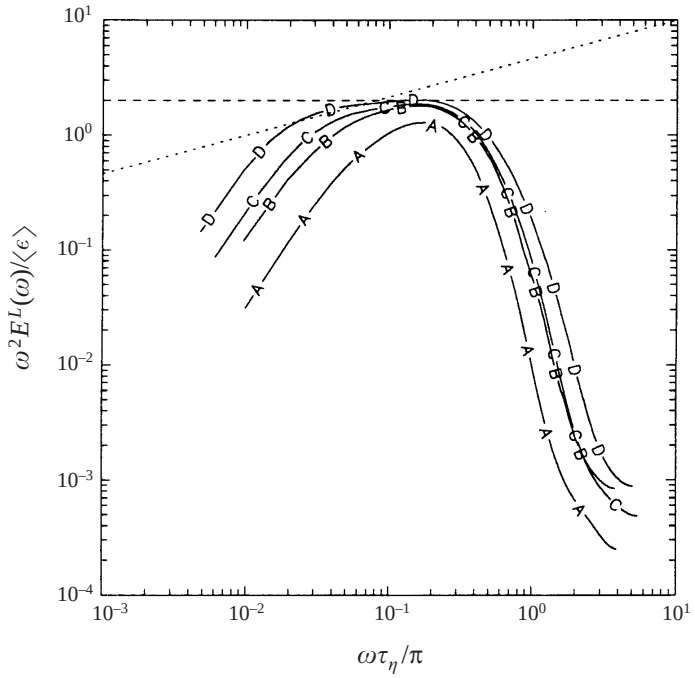

FIGURE 5. Lagrangian frequency spectrum of velocity, in Kolmogorov scaling. Lines A to D are for the 64^3, 128^3, 256^3 and 512^3 simulations respectively. The dashed line is drawn at the level 2.0, and the dotted line is one of slope 1/3.

$C_K \approx 1.62$ (Sreenivasan 1995; Yeung & Zhou 1997) this yields $B \approx 2.06$ which is evidently in good agreement with data in figure 5. It is recognized, of course, that because of the limited range of scales in DNS, a strong claim of inertial-range scaling cannot be made. Nevertheless, it is interesting to note that if an infinitely wide inertial-range is assumed then this value of B suggests an estimate for the inertial-range constant C_0 in the Lagrangian structure function (Monin & Yaglom 1975, p. 539) as $2.06\pi = 6.47$, which is remarkably close to the asymptotic value of about 7 suggested by Sawford (1991).

The high-frequency part of the Lagrangian frequency spectrum is, apart from possible contamination from numerical noise associated with a finite sampling time interval (h, which is about 1/5 of τ_η), determined by changes of the particle velocity during short periods of time. The latter is, of course, given by the fluid particle acceleration, which has been shown to deviate from classical Kolmogorov scaling in related computations (Vedula & Yeung 1999). The curves in figure 5 have a slight turn-up at the high-frequency end, suggesting a noise level similar to that in Yeung & Pope (1989), where procedures for noise control were discussed at length. However, despite this presence of noise, it can still be said that the data show no tendency of a 'collapse' with increasing Reynolds number. It should be noted that, because of differences between Lagrangian and Eulerian frames of reference, this apparent non-universality in the Lagrangian frequency domain does not contradict the well-known universality of the Eulerian spectrum at high wavenumbers.

As suggested by a referee, it would be of interest to compare the scaling observed in figure 5 with that for the *Eulerian* frequency spectrum, for which an $\omega^{-5/3}$ form was proposed by Tennekes (1975). Unfortunately, since we have not saved the required Eulerian time series (at fixed points) for the highest two Reynolds numbers in this

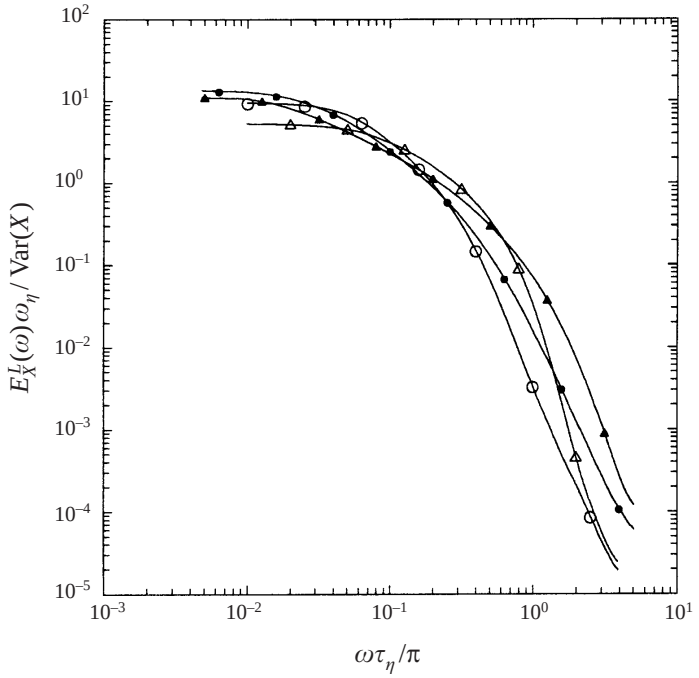

FIGURE 6. Normalized Lagrangian frequency spectra of energy dissipation (triangles) and enstrophy (circles), versus Kolmogorov-scaled frequency. Open symbols for data from the 64^3 simulation, closed symbols for 512^3. (On the y-axis the symbol X denotes either ϵ or ω^2 as random variables, of variance $\mathrm{Var}(X)$.)

work, this issue cannot be addressed reliably here. The dotted line of slope 1/3 in figure 5 (with $\omega^2 E^L(\omega)$ being actually plotted) does suggest that evidence for $\omega^{-5/3}$ is weaker than that for ω^{-2} in the Lagrangian spectrum.

In figure 6 we compare the Lagrangian frequency spectra for energy dissipation and enstrophy in dimensionless form, using data at the lowest and highest Reynolds numbers in the simulation. All of the curves display a plateau at the low-frequency end and a steady drop at high frequencies. Compared to enstrophy, the energy dissipation has more high-frequency content, which is consistent with results in Yeung & Pope (1989, figure 7) and is perhaps due to a more important role of high-frequency but low-magnitude changes in the dissipation time series. (It may be noted that (Chen, Sreenivasan & Nelkin 1997) differences between dissipation and enstrophy are also observed in their Eulerian spatial structure.) At higher Reynolds numbers the curves shown are generally shifted to larger magnitudes and higher frequencies. It should be noted that for a stationary variable the value of its frequency spectrum at zero frequency is proportional to its integral time scale. With the current choice of normalization factors this implies that the heights of the low-frequency plateaus in this figure are given by twice the ratios between the corresponding integral time scales (of ϵ or ω^2) and the Kolmogorov time scale. The data in table 2 show that the ratios $\mathscr{T}_\epsilon/\tau_\eta$ and $\mathscr{T}_{\omega^2}/\tau_\eta$ indeed increase with Reynolds number.

4.2. *Single-scalar results*

Here we first consider the one-time statistics of the total scalar value ($\tilde{\phi}^+$) and the scalar fluctuation (ϕ^+) following fluid particles, to be followed by two-time correlations and the properties of scalar gradients and dissipation.

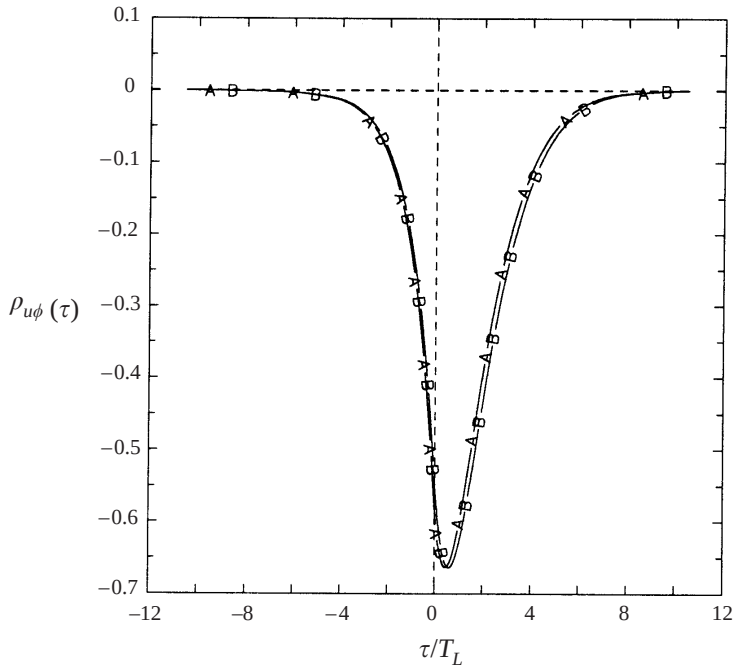

FIGURE 7. Lagrangian velocity–scalar cross-correlation function, taken from the 512^3 simulation, for scalars at $Sc = 1/8$ (A) and $Sc = 1$ (B).

Upon noting that displacement is the time integral of velocity we can re-write (3) as

$$\tilde{\phi}^+(t) = Gx^+(0) + G\int_0^t u^+(t')\,\mathrm{d}t' + \phi^+(t). \tag{9}$$

Since both $u^+(t)$ and $\phi^+(t)$ are stationary random variables of zero mean, we obtain immediately

$$\langle\tilde{\phi}^+(t)\rangle = G\langle x^+(0)\rangle, \tag{10}$$

which is simply fixed by the chosen distribution of initial particle positions. (Note on notation: depending on context, angled brackets in this paper may represent averaging over either Lagrangian or Eulerian samples.) However, $\tilde{\phi}^+$ is not stationary in time. In fact, taking the variance of each side of (9) gives

$$\mathrm{Var}(\tilde{\phi}^+) = \mathrm{Var}(\phi^+) + G^2\mathrm{Var}(x^+(0)) + 2G\int_0^t \langle\phi^+(t)u^+(t')\rangle\mathrm{d}t' + G^2\int_0^t\int_0^t \langle u^+(t')u^+(t'')\rangle\mathrm{d}t'\,\mathrm{d}t'', \tag{11}$$

where time dependence is expressed via two integrals of Lagrangian correlations. The integrand in the first integral is shown in figure 7 as the normalized velocity–scalar cross-correlation function, $\rho_{u\phi}(\tau)$. Clearly, this cross-correlation is predominantly negative, and significantly stronger for positive time lags which in our definition (see (6)) corresponds to the correlation between velocity at time t and scalar at a later time $t + \tau$ ($\tau > 0$). This asymmetry is consistent with the idea that the scalars are passively transported by the velocity field, in that the velocity at one time instant can have a definite causative effect on the scalar fluctuation for a short time interval

Grid	64^3	64^3	64^3	128^3	128^3	128^3	256^3	256^3	512^3	512^3
Sc	1/4	1/2	1	1/8	1/4	1	1/8	1	1/8	1
$\rho(u,\phi)$	−0.639	−0.595	−0.551	−0.587	−0.557	−0.499	−0.563	−0.510	−0.595	−0.559
r_ϕ	2.826	2.254	1.843	3.740	3.253	2.548	3.188	2.447	2.746	2.376
$\rho(\nabla u,\nabla\phi)$	−0.456	−0.379	−0.305	−0.291	−0.254	−0.175	−0.234	−0.137	−0.135	−0.079
A	−0.542	−0.357	−0.225	−0.426	−0.282	−0.110	−0.371	−0.088	−0.230	−0.051
a	−1.104	−1.219	−1.258	−1.145	−1.222	−1.259	−1.159	−1.291	−1.336	−1.413
b	−0.163	−0.368	−0.469	−0.246	−0.399	−0.518	−0.282	−0.571	−0.564	−0.739
$-b/a$	−0.148	−0.302	−0.373	−0.215	−0.327	−0.412	−0.243	−0.442	−0.422	−0.523
$\rho_E(\nabla u,\nabla\phi)$	−0.442	−0.373	−0.301	−0.306	−0.267	−0.183	−0.239	−0.140	−0.138	−0.081

TABLE 3. Parameters in the estimation of velocity–scalar conditional diffusion. The Lagrangian value of $\rho(\nabla u,\nabla\phi)$ is used to obtain the model coefficients. The Eulerian value (ρ_E) is shown at the bottom.

later, but not vice versa. The effects of Schmidt number are weak, although it can be seen that the asymmetry discussed here is stronger at higher Schmidt number. The value of this cross-correlation at $\tau = 0$, i.e. the velocity–scalar correlation coefficient ($\rho(u,\phi)$), is listed in table 3 together with other parameters to be discussed below. It should be noted that the sign of $\rho(u,\phi)$ is opposite to that of the mean scalar gradient in the chosen coordinate system, such that (in this work, and as in most situations) the turbulent scalar flux ($\langle u\phi\rangle$) is essentially a gradient transport effect for the mean scalar field.

At sufficiently large times the first integral in (11) ultimately converges, so that the mean-squared particle displacement becomes the dominant contribution. At times $t \gg T_L$ it is well known that (Taylor 1921)

$$\int_0^t\int_0^t \langle u^+(t')u^+(t'')\rangle \mathrm{d}t'\,\mathrm{d}t'' \approx 2u'^2 T_L t, \tag{12}$$

which in turn implies linear growth for $\mathrm{Var}(\tilde{\phi})$ in this regime.

Although $\tilde{\phi}^+(t)$ is not stationary, it can be treated as a random process with stationary increments. This can be seen by writing (from (3)) the increment $\Delta_\tau\tilde{\phi}^+ \equiv \tilde{\phi}^+(t+\tau) - \tilde{\phi}^+(t)$ as

$$\Delta\tau\tilde{\phi}^+ = G(x^+(t+\tau) - x^+(t)) + (\phi^+(t+\tau) - \phi^+(t)), \tag{13}$$

where the first bracket on the right is also equal to $\int_t^{t+\tau} u^+(t')\,\mathrm{d}t'$. Stationarity of the fluctuations $\phi^+(t)$ and $u^+(t)$ implies that their respective contributions to (13) depend on the time increment τ only (but not on t).

In a way similar to Eulerian structure functions for spatial structure, the properties of Lagrangian increments are important descriptors of the temporal structure of the turbulence. Stationarity in the fluctuations implies that only even-order moments of $\Delta\tau\tilde{\phi}^+$ can have non-trivial values. For the second moment it should be noted that, because of a correlation between velocity and scalar fluctuations at different times, the two contributions on the right-hand side of (13) are not independent. In fact, by applying a time shift and a change of variables their covariance

$$G\int_t^{t+\tau} \langle u^+(t')(\phi^+(t+\tau) - \phi^+(t))\rangle\,\mathrm{d}t'$$

can be written as

$$G\sigma_\phi\sigma_u \int_{-\tau/2}^{\tau/2} [\rho_{u\phi}(\tau/2 - t') - \rho_{u\phi}(t' - \tau/2)]\ \mathrm{d}t' \tag{14}$$

(where σ_ϕ and σ_u denote r.m.s. fluctuations). Clearly, asymmetry in the velocity–scalar cross-correlation noted in figure 7 plays an essential role in this integral.

For a non-dimensional measure of the shape of the PDF of $\Delta\tau\tilde{\phi}^+$ we can consider its flatness factor, compared with the Gaussian value of 3.0. Figure 8(a, b) shows the data for different Reynolds and Schmidt numbers, as a function of time lag which is normalized by the Kolmogorov time scale in (a) and the Lagrangian integral time scale in (b). At small τ it can be seen that $\Delta\tau\tilde{\phi}^+$ is highly intermittent, with large flatness factors. This can be understood by recognizing that in the small time limit ($\tau \ll \tau_\eta$) use of (2) leads to

$$\Delta\tau\tilde{\phi}^+ \approx \tau\frac{\mathrm{d}\tilde{\phi}^+}{\mathrm{d}t} = \tau\frac{\mathrm{D}\tilde{\phi}}{\mathrm{D}t} = \tau D_\phi\nabla^2\phi \tag{15}$$

which implies that the limiting flatness factor of $\Delta\tau\tilde{\phi}^+$ should be close to that of the Laplacian of the scalar fluctuations in space. On the other hand at large time lags both contributions in (13) become close to Gaussian, with figure 8(b) showing that this requires at least several integral time scales.

The results in figure 8(a, b) can be used as a stringent fourth-moment test for stochastic modelling, with special interest in the range of intermediate time lags. While it is also tempting to try to infer scaling relations for time lags in the inertial range $\tau_\eta \ll \tau \ll T_L$, this is limited by the fact that even in the 512^3 simulation the ratio T_L/τ_η is only 20 (table 2). It is clear, however, that the scalar increment is far from Gaussian at intermediate τ: e.g. for $Sc = 1$ in the 512^3 simulation this flatness factor is about 8 at $\tau/\tau_\eta \approx 4$, which in this case corresponds to $\tau/T_L \approx 0.2$.

In stochastic modelling a Markovian assumption is often made, which in the present context amounts to attempting to predict the 'future' value $\tilde{\phi}^+(t + \tau)$ (especially for small positive τ) conditioned or based upon knowledge of the 'current' value $\tilde{\phi}^+(t)$. Because of the strong role of advective transport by the velocity fluctuations, it is important to include conditioning upon both the velocity and scalar (Fox 1996; Pope 1998), corresponding to an unclosed term in the transport equation for velocity–scalar joint PDFs. In view of (15) there is thus great interest in the conditional expectation $\langle D_\phi(\nabla^2\phi)^+|u^+, \phi^+\rangle$, which we refer to as the velocity–scalar conditional diffusion. Because of homogeneity, this is the same as the Eulerian quantity $\langle D_\phi\nabla^2\phi|u, \phi\rangle$ which is more conveniently evaluated by drawing samples at each grid point. More details on the estimation of conditional expectations and sampling issues are given in Yeung (1998).

For the purpose of modelling it is useful to develop a linear regression estimate for the conditional diffusion. Following Overholt & Pope (1996, also adopted for related quantities in Yeung 1998) we suppose that the fluctuations of $\nabla^2\phi$ are given in non-dimensional form by

$$\frac{D_\phi\nabla^2\phi}{\langle\chi\rangle/2\sigma_\phi} = a\frac{\phi}{\sigma_\phi} + b\frac{u}{\sigma_u} + \xi, \tag{16}$$

where ξ is a random term uncorrelated with the turbulent fluctuations (ϕ and u) and

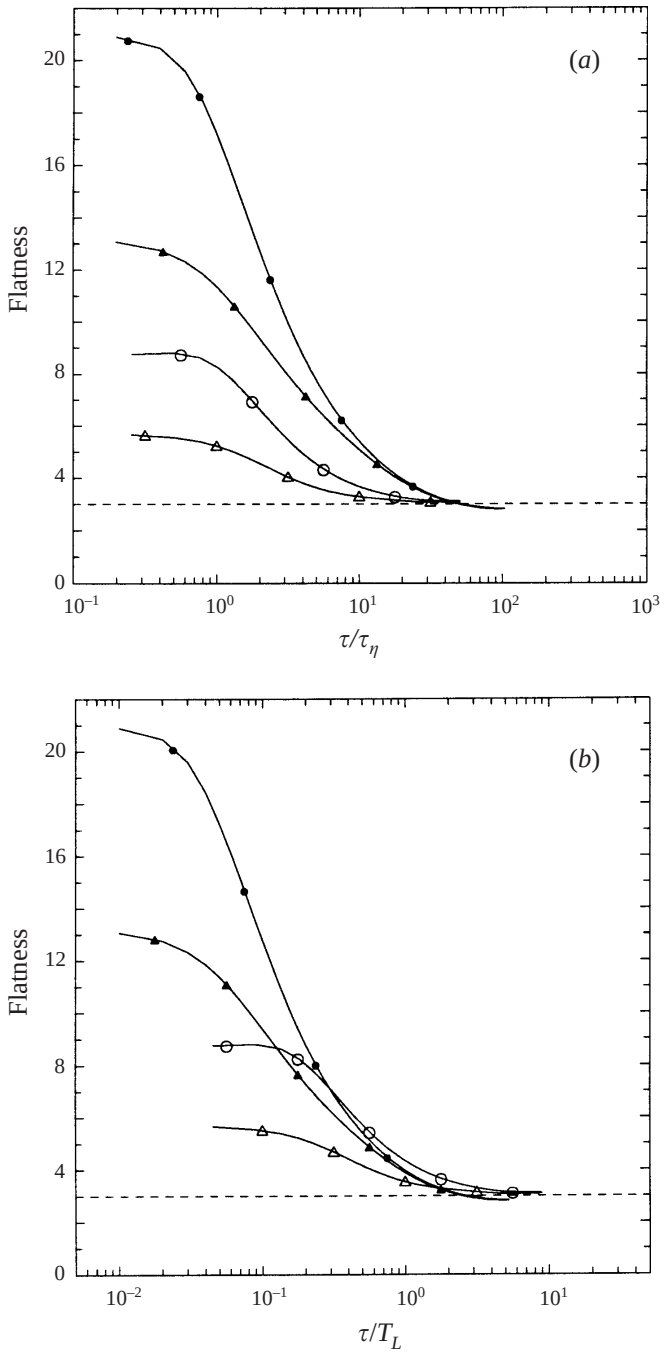

FIGURE 8. Flatness factor of Lagrangian temporal increment of *total* scalar ($\tilde{\phi}^+$), with time lag normalized by (*a*) the Kolmogorov time scale and (*b*) the Lagrangian integral time scale: $Sc = 1/4$ ($\triangle$) and $Sc = 1$ ($\bigcirc$) from 64^3 simulation; corresponding closed symbols for $Sc = 1/8$ and $Sc = 1$ respectively from 512^3.

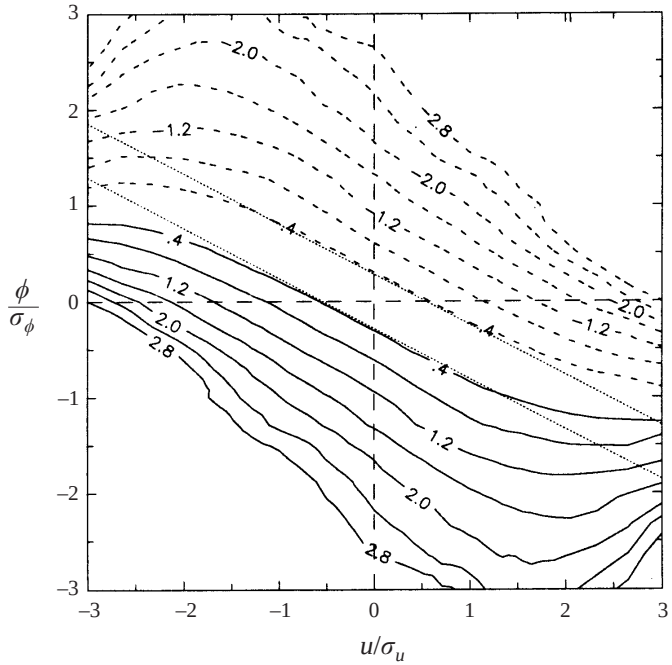

FIGURE 9. Contour plot of the conditional diffusion for velocity and scalar, from Eulerian data on the 512^3 grid, $Sc = 1$. Dotted lines give contour levels of ± 0.4 from linear regression estimate (18).

the coefficients a and b can be expressed solely in terms of the parameter

$$\Lambda = \frac{2D_\phi \sigma_\phi}{\sigma_u \langle \chi \rangle} \left\langle \frac{\partial u}{\partial x_i} \frac{\partial \phi}{\partial x_i} \right\rangle, \tag{17}$$

where $\langle \chi \rangle$ is the mean scalar dissipation rate. The solution from linear regression analysis for a and b can be written as

$$\frac{D_\phi \langle \nabla^2 \phi | u, \phi \rangle}{\langle \chi \rangle / 2\sigma_\phi} = \frac{1 - \Lambda \rho_{u\phi}}{\rho_{u\phi}^2 - 1} \left(\frac{\phi}{\sigma_\phi} \right) + \frac{\Lambda - \rho_{u\phi}}{\rho_{u\phi}^2 - 1} \left(\frac{u}{\sigma_u} \right). \tag{18}$$

Whereas Overholt & Pope (1996) reported that the coefficients vary only weakly with Reynolds number, here we attempt to clarify dependences on Reynolds and Schmidt numbers using DNS results spanning a wider parameter range. By assuming isotropy for the velocity field and using the definition of $\langle \chi \rangle$ we can re-write (17) as

$$\Lambda = \rho(\nabla u, \nabla \phi) Sc^{-1/2} r_\phi^{-1/2} \tag{19}$$

where $\rho(\nabla u, \nabla \phi)$ is the correlation coefficient between the vectors ∇u and $\nabla \phi$, and

$$r_\phi \equiv \frac{K}{\langle \epsilon \rangle} \Big/ \frac{\langle \phi^2 \rangle}{\langle \chi \rangle} \tag{20}$$

is the mechanical-to-scalar time-scale ratio often discussed in the literature on turbulent mixing (e.g. Eswaran & Pope 1988*b*) and sometimes used as an empirical parameter in modelling (Fox 1995, 1996).

Numerical values of parameters appearing in (16)–(20) are displayed in table 3. At each Reynolds number all of the quantities shown exhibit a systematic dependence on Schmidt number. In particular at higher Sc the velocity and scalar fields are less

correlated in both the respective fluctuations and their gradients. Lagrangian values of $\rho(\nabla u, \nabla\phi)$ are used to compute Λ, a, b and are seen to be close to Eulerian values included in the table. A non-zero value of $\rho(\nabla u, \nabla\phi)$ is an indication of departures from local isotropy for the scalar field, which has been questioned in the literature (Sreenivasan 1991; Warhaft 2000). The observed departures from local isotropy are clearly significant, but also become weaker at higher R_λ and Sc where a wider range of scales in the scalar fluctuations is expected. The time-scale ratio r_ϕ is seen to decrease with Schmidt number, primarily through changes in the scalar variance since the scalar dissipation becomes dominated by transfer from the large scales and hence insensitive to changes in molecular diffusivity.

Figure 9 shows a contour plot of the conditional diffusion ($D_\phi\langle\nabla^2\phi|u,\phi\rangle$) from the 512^3 data for $Sc = 1$, based on an ensemble average taken over multiple velocity and scalar fields saved during the simulation. Because of considerable noise which limits the reliability of results in low-probability regions we show only contour lines falling in the inner regions of the sampling envelope. Subject to this caveat, it can be seen that the interior contour lines are approximately linear, and are in good agreement with the linear regression result of (19) which is represented by dotted lines of slope $-b/a$. The relationship between a linear form for the conditional diffusion and the Gaussianity of velocity and scalar fluctuations has been addressed in Yeung (1998, with a detailed analysis in the Appendix). For larger velocity or scalar fluctuations there appear to be some deviations from a linear form, which cannot be ascertained perfectly from the data but (as in figure 7 of Yeung 1998) may be due to a slight non-Gaussianity in the tails of velocity or scalar PDFs. The magnitude of the slope $-b/a$ is essentially a measure of the relative sensitivities of the conditional diffusion to local velocity and scalar fluctuations. The numerical values in table 3 also suggest that the influence of the velocity (hence advective transport) becomes stronger at increasing values of R_λ and Sc.

We now turn our attention to the Lagrangian properties of the scalar fluctuations, $\phi^+(t)$. Figure 10 shows the autocorrelation functions of the scalars and their dissipation rates in the 512^3 simulation, compared with those of the velocity and energy dissipation. It is clear that the scalar fluctuations remain correlated the longest, especially at higher Schmidt number. This observation is consistent with the increasing dominance of advective transport, since in the limit $Sc \to \infty$ (zero diffusivity but with viscosity remaining finite) the scalar would behave as a non-diffusive material property that is invariant along the fluid particle trajectories and hence have infinite correlation time. On the other hand the scalar dissipation is seen to de-correlate rapidly, although for very short time lags ($\tau/T_L \leqslant 0.1$, in the inset) this de-correlation is slightly less rapid than that for the energy dissipation. The similarity between the curves for energy dissipation and scalar dissipation at early time lags does suggest that the small-scale motions play an essential role. Yet beyond this time lag the scalar dissipation drops much faster than the energy dissipation, with only a very weak dependence on Schmidt number.

Our present interest in the autocorrelation functions discussed above is in part motivated by their important role in the Lagrangian stochastic modelling of turbulent mixing. In particular recent work by Fox (1997, 1999) predicts that the scalar fluctuations vary very smoothly in time (and hence have long integral time scales), and that the Lagrangian time series of the scalar dissipation has longer time scales than the energy dissipation. Whereas the first of these results is supported by the DNS data, the second is not. The newly available Lagrangian information from DNS is expected to be useful for improvements in modelling (Yeung & Fox 1999).

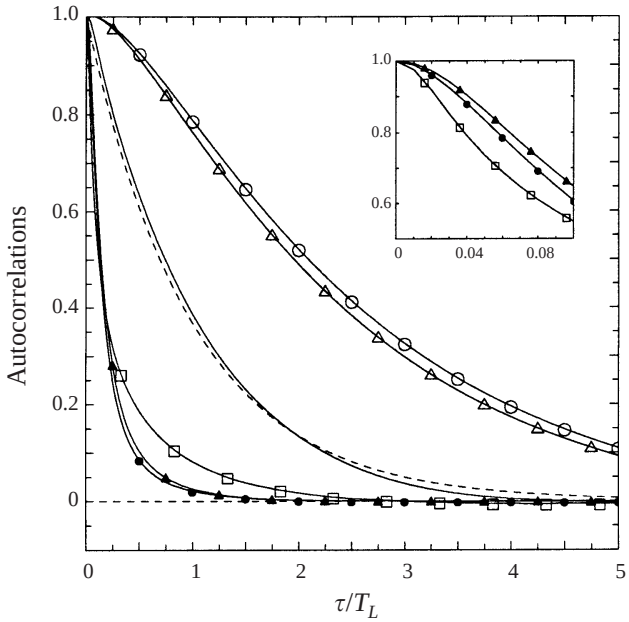

FIGURE 10. Lagrangian autocorrelations from the 512^3 simulation: velocity (unmarked solid line), energy dissipation (□), scalar ϕ_1 at $Sc = 1/8$ (△), scalar ϕ_2 at $Sc = 1$ (○), dissipation of ϕ_1 (▲), and dissipation of ϕ_2 (●). The dashed curve shows the exponential approximation to the velocity autocorrelation. Energy and scalar dissipation autocorrelations at very small time lags ($\tau/T_L \leqslant 0.1$) are shown magnified in the inset.

In figure 10 we have shown only results from the simulation at the highest Reynolds number. The complete set of results on integral time-scale ratios (normalized by T_L) is given in table 4 for all Reynolds and Schmidt numbers in the simulations. For scalars ratio $\mathscr{T}_\phi/T_L$ is generally of order 2, which is broadly in line with expectations based on simple models (S. B. Pope 2000, personal communication). There is, however, and despite some erratic values in the 256^3 case, a weak overall increase in $\mathscr{T}_\phi/T_L$ with both R_λ and Sc. In contrast, the integral time-scale ratios for scalar gradients (which are computed separately for components parallel and perpendicular to the imposed mean gradient) show a strong decrease with both R_λ and Sc. Differences between the vector components $\nabla_\parallel\phi$ and $\nabla_\perp\phi$ apparently weaken with increasing R_λ and Sc. A 'componentiality effect' similar to that discussed for vorticity and enstrophy in § 4.1 is evident in the progression from the square of one scalar gradient component, to the sum of squares of two coordinate components (written as $2(\nabla_\perp\phi)^2$), and finally to the scalar dissipation in three dimensions. Furthermore, as the Reynolds number increases, the scalar dissipation time scale is seen to decrease relative to that for the energy dissipation.

If a given stationary random process is first-order Markovian its autocorrelation would be determined by the integral time scale ($\mathscr{T}$) alone, in the form $\exp(-\tau/\mathscr{T})$. For Lagrangian fluctuations in turbulence this cannot be strictly true, since their differentiability in time implies a quadratic decrease instead at small time lags. Nevertheless in practice as a test of Markovian character it is of interest to compare the observed autocorrelations with the exponential. Figure 11(a,b) shows such a comparison for velocity and scalar fluctuations at the lowest and highest Reynolds numbers in the simulations. For both velocity and scalars we find that the exponential

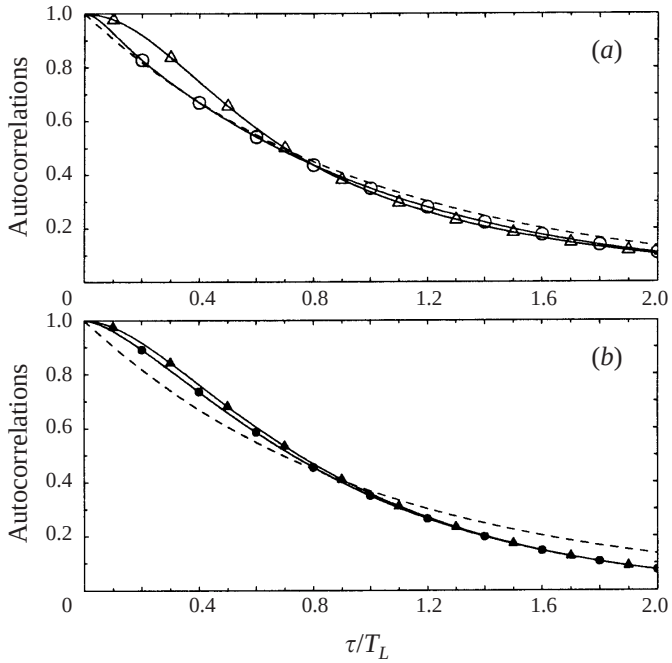

FIGURE 11. Lagrangian autocorrelations for (*a*) velocity and (*b*) scalar at $Sc = 1$ with time lags normalized by their respective integral time scales ($\mathscr{T}$), from the 64^3 (triangles) and 512^3 (circles) simulations. Dashed line shows the exponential approximation corresponding to the first-order Markov processes of the same integral time scale.

Grid	64^3	64^3	64^3	128^3	128^3	128^3	256^3	256^3	512^3	512^3
Sc	1/4	1/2	1	1/8	1/4	1	1/8	1	1/8	1
$\mathscr{T}_\phi/T_L$	1.89	2.03	2.17	1.97	2.04	2.19	1.73	1.88	2.22	2.33
$\mathscr{T}_{\nabla_\parallel\phi}/T_L$	0.605	0.558	0.516	0.479	0.410	0.320	0.384	0.258	0.264	0.170
$\mathscr{T}_{\nabla_\perp\phi}/T_L$	0.777	0.654	0.566	0.579	0.461	0.335	0.446	0.267	0.297	0.174
$\mathscr{T}_{(\nabla_\parallel\phi)^2}/T_L$	0.416	0.406	0.412	0.305	0.287	0.284	0.263	0.241	0.193	0.172
$\mathscr{T}_{2(\nabla_\perp\phi)^2}/T_L$	0.423	0.413	0.425	0.333	0.302	0.296	0.280	0.250	0.208	0.185
$\mathscr{T}_\chi/T_L$	0.459	0.468	0.498	0.350	0.323	0.325	0.300	0.279	0.228	0.208
$\mathscr{T}_\chi/\mathscr{T}_\epsilon$	0.922	0.940	1.000	0.873	0.805	0.810	0.831	0.773	0.770	0.703

TABLE 4. Integral time scales of scalar field parameters.

becomes a better approximation at higher Reynolds number. However, the approach to Markovian behaviour appears to be weaker for the scalars, which suggests that non-Markovian modelling (e.g. Durbin 1980; Fung & Vassilicos 1998 for dispersion between fluid particle pairs, which is related to scalar variance) may have advantages.

Whereas the DNS data have provided clear evidence that scalar fluctuations have longer Lagrangian time scales than the velocity, it is worth noting that the opposite is true when time scales based on Eulerian one-point statistics are considered – such as via the ratio r_ϕ defined in (20). To understand these differences in greater detail it is useful to compare the statistics of the Lagrangian and Eulerian rates of change, which are respectively defined by the material derivative ($\mathrm{D}/\mathrm{D}t$) and unsteady time derivative ($\partial/\partial t$) operators. The first of these is conveniently obtained by a simple

second-order finite difference in time for $\phi^+(t)$, provided the sampling interval h (see table 1) is sufficiently small. The second requires, in principle, evaluation from *Eulerian* time series of fluctuations recorded at fixed (grid) points in space, which we have not saved in our higher resolution runs. However, it is possible to recover the unsteady time derivative at the fluid particle position from Lagrangian time series of velocity, scalar and scalar gradients, using the relation

$$\frac{\partial \phi}{\partial t} = \frac{\mathrm{D}\phi}{\mathrm{D}t} - u_i \frac{\partial \phi}{\partial x_i}. \tag{21}$$

Basically, we evaluate the advective term from the Lagrangian time series, and use it to recover samples of the unsteady time derivative $\partial\phi/\partial t$ at randomly located instead of fixed sampling locations. Because of homogeneity, the statistics obtained are essentially equivalent. From the statistics of the respective time derivatives we can define Lagrangian and Eulerian 'Taylor' time scales as

$$\tau_{L,\phi} = \left[\frac{\langle \phi^2 \rangle}{\langle (\mathrm{d}\phi^+/\mathrm{d}t)^2 \rangle}\right]^{/1/2}, \qquad \tau_{E,\phi} = \left[\frac{\langle \phi^2 \rangle}{\langle (\partial\phi/\partial t)^2 \rangle}\right]^{/1/2} \tag{22}$$

and compare these with each other. (Corresponding time scales for the velocity were studied by Tennekes 1975.)

Table 5 shows the data for $\tau_{L,\phi}$ and $\tau_{E,\phi}$, normalized by the Kolmogorov time scale. The normalized values of $\tau_{L,\phi}$ show little dependence on Schmidt number but those for $\tau_{E,\phi}$ decrease strongly with Schmidt number. Comparison between scalars of the same Schmidt number (e.g. $Sc = 1/4$ on 64^3 and 128^3 grids, or $Sc = 1/8$ on 128^3, 256^3 and 512^3 grids) shows that an increase in Reynolds number causes a systematic increase in $\tau_{L,\phi}/\tau_\eta$ but a decrease in $\tau_{E,\phi}/\tau_\eta$. It should be noted that the ratio $\tau_{L,\phi}/\tau_{E,\phi}$ is the inverse square root of the ratio between the variances of the corresponding time derivatives. Consequently we can conclude that the difference between Eulerian and Lagrangian rates of change becomes more pronounced at higher Reynolds and Schmidt numbers. This result also implies that the difference between these two derivative operators – i.e. advective transport by the velocity fluctuations – becomes increasingly dominant.

Unlike the case for the velocity, the Lagrangian frequency spectrum of scalars has received little attention in the literature. The Eulerian *wavenumber* spectrum is better known: for $Sc \leqslant 1$ at sufficiently high Reynolds number the Obukhov–Corrsin similarity theory for an inertial–convective subrange gives $E_\phi(k) \sim \langle\chi\rangle\langle\epsilon\rangle^{-1/3}k^{-5/3}$ at intermediate wavenumbers which is generally supported by experiment (Sreenivasan 1996; Mydlarski & Warhaft 1998). However if we consider a scaling law of the type $E^L_\phi(\omega) \sim \langle\chi\rangle^a\langle\epsilon\rangle^b\omega^c$ for the Lagrangian spectrum at intermediate frequencies we find that the exponent b must be zero because of dimensional reasons. We obtain

$$E^L_\phi(\omega) \sim \langle\chi\rangle\omega^{-2} \quad (\pi/T_L \ll \omega \ll \pi/\tau_\eta). \tag{23}$$

Clearly, data at high Reynolds number are required to test this 'hypothesis', as well as to estimate the value of the implied proportionality constant, which we may denote as B_ϕ in analogy to (8).

Figure 12 shows DNS data at the lowest and highest Reynolds numbers for the scalar frequency spectra, in the form $\omega^2 E^L_\phi(\omega)$ versus the Kolmogorov-scaled frequency. The data suggest that B_ϕ is of order 0.5 or slightly higher. However, the evidence for a 'plateau' is considerably weaker than that for the velocity (figure 5). In addition, the peak of the normalized spectrum increases with Schmidt number whereas its location shifts towards lower frequencies at higher Reynolds numbers.

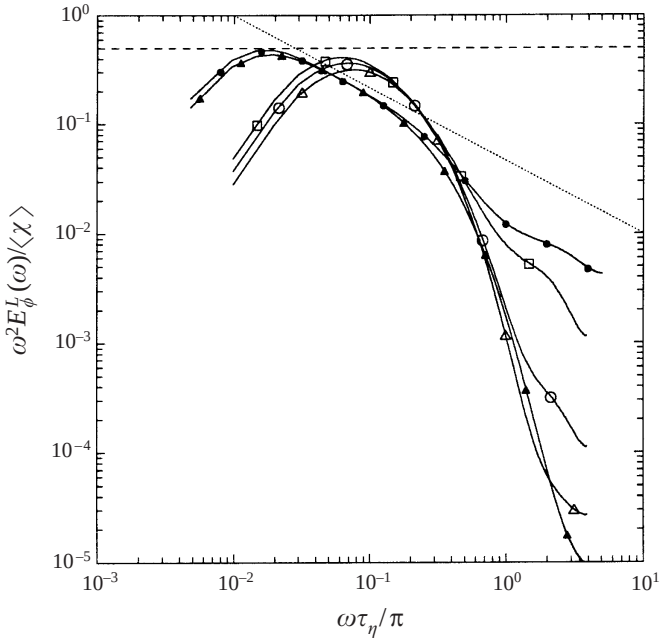

FIGURE 12. Lagrangian frequency spectra of scalars normalized by Kolmogorov variables: $Sc = 1/4$ (△), $1/2$ (○), and 1 (□) from the 64^3 simulation, compared with $Sc = 1/8$ (▲) and $Sc = 1$ (●) in the 512^3 simulation. The dotted line is of slope $-2/3$.

Grid	64^3	64^3	64^3	128^3	128^3	128^3	256^3	256^3	512^3	512^3
Sc	1/4	1/2	1	1/8	1/4	1	1/8	1	1/8	1
$\tau_{L,\phi}/\tau_\eta$	4.95	5.26	5.40	7.79	7.97	7.89	9.56	9.29	13.55	12.33
$\tau_{E,\phi}/\tau_\eta$	3.19	2.46	1.89	3.86	2.77	1.47	3.57	1.35	3.41	1.22
$\tau_{L,\phi}/\tau_{E,\phi}$	1.55	2.13	2.85	2.02	2.88	5.35	2.68	6.87	3.97	10.11

TABLE 5. Lagrangian and Eulerian Taylor time scales for scalar fluctuations.

For these reasons the estimate $B_\phi \sim 0.5$ should be interpreted as merely suggestive and subject to further investigations. Incidentally, the 512^3 data for both Schmidt numbers also show an $\omega^{-8/3}$ (dotted line, after dividing by ω^2) scaling range of more than half a decade. However, this observation is not understood and should be subjected to further verification or interpretation in the future.

At a given Reynolds number the Schmidt number dependence in figure 12 is significant mainly at low and high frequencies. It should be noted that the frequency spectrum at zero frequency is proportional to the integral time scale. The increase with Sc at low frequencies is thus consistent with the variation of scalar integral time scales shown in table 4. At high frequencies one expects the spectrum to drop off with frequency more slowly at higher Schmidt numbers. Whereas this trend is indeed observed in figure 12 the significant change of spectral slope at high frequencies for scalars of higher Sc suggests that the results are influenced by numerical noise. The most likely source of this noise is interpolation error for the Lagrangian scalar fluctuation which is expected to be more significant for less-diffusive scalars of greater high-wavenumber spectral content (see also figure 1*d*).

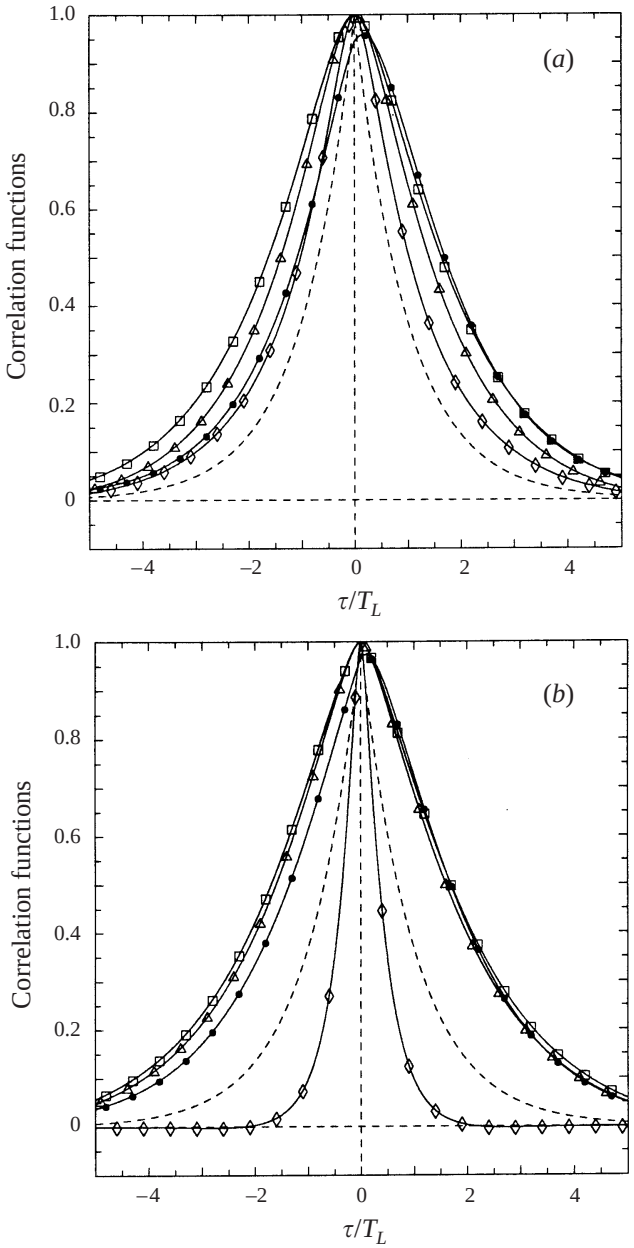

FIGURE 13. Lagrangian autocorrelations of scalar fluctuations ϕ_α (△), ϕ_β (□), their difference $z = \phi_\alpha - \phi_\beta$ (◇), and cross-correlation function ($\rho_{\alpha\beta}(\tau)$, ●), for scalars with (*a*) the $Sc = (1/4, 1)$ from the 64^3 simulation and (*b*) $Sc = (1/8, 1)$ from the 512^3 simulation. The dashed curve shows the exponential approximation to the velocity autocorrelation.

It can be seen from figure 12 that the peak of the Lagrangian scalar spectrum (without the ω^2 factor) lies at the lowest frequencies. The same is true for the spectrum of scalar dissipation (not shown), which has a low-frequency plateau resembling that seen for the energy dissipation in figure 6.

Grid	64^3	64^3	64^3	128^3	128^3	128^3	256^3	512^3
Sc_α, Sc_β	1/4,1/2	1/4,1	1/2,1	1/8,1/4	1/8,1	1/4,1	1/8,1	1/8, 1
$\mu_4(z)$	3.57	3.60	3.70	4.26	4.24	4.37	4.64	6.04
$\mathscr{T}_z/T_L$	1.41	1.48	1.42	0.86	0.96	0.89	0.77	0.46
$\tau_{L,z}/\tau_\eta$	2.98	2.94	2.56	3.02	3.16	2.73	3.39	3.02
ρ_L	0.919	0.703	0.896	0.914	0.451	0.643	0.455	0.402

TABLE 6. Two-scalar statistics from Lagrangian data: flatness factor (μ_4), Lagrangian integral and Taylor time scales for $z \equiv \phi_\alpha - \phi_\beta$, and correlation ρ_L between the Lagrangian time derivatives of different scalars.

4.3. *Two-scalar statistics and differential diffusion*

In studies of differential diffusion between two scalars $(\phi_\alpha, \phi_\beta)$ the emphasis is on their joint statistical properties. Important quantities include cross-correlations at the second-moment level, and the statistics of the difference $z = \phi_\alpha - \phi_\beta$ (e.g. flatness factors for intermittency, in table 6), which is more directly relevant in combustion or unsteady mixing problems (e.g. Kronenburg & Bilger 1997).

The Lagrangian cross-correlation function between two scalars at two different times is defined by

$$\rho_{\alpha\beta}(\tau) = \frac{\langle \phi_\alpha^+(t)\phi_\beta^+(t+\tau)\rangle}{\sigma_\alpha \sigma_\beta}; \tag{24}$$

in general it is not an even function of τ but has the property that

$$\rho_{\beta\alpha}(\tau) = \rho_{\alpha\beta}(-\tau). \tag{25}$$

Although the autocorrelation of the difference (z) can, in principle, be expressed in terms of one- and two-scalar correlations, the relation involved is numerically ill-conditioned at small τ, and also subject to large sampling uncertainties at large τ. Instead, we form the difference z from the raw time series (of ϕ_α^+ and ϕ_β^+) and compute its autocorrelation directly.

In figure 13(a, b) we show one- and two-scalar correlations together with the autocorrelation of their difference, the latter being computed directly from the Lagrangian time series of $z^+(t)$. The Schmidt number combinations in parts (a) and (b) of this figure are selected to represent cases of respectively the strongest and weakest effects of differential diffusion in the simulations. The ordering within each pair is such that the first scalar (ϕ_α) is more diffusive (or of lower Sc). Whereas all autocorrelations (of ϕ_α, ϕ_β, z) are by definition even functions of τ the cross-correlation displays clear asymmetry, being stronger for positive than negative values of τ. Since the two scalars would have the same properties if their diffusivities were equal, this asymmetry can be regarded as a measure of differential diffusion. Indeed, in figure 13(b) where a value of $\rho_{\alpha\beta}(0)$ closer to unity signifies weaker differential diffusion the cross-correlation curve is correspondingly less asymmetric.

Given that the scalars considered (being non-reactive) do not have direct causative effects on one another, the physical reasons for this asymmetry are subtle. However, this can be traced to the fact that the differences between the Lagrangian rates of change of ϕ_α and ϕ_β lie in their rates of molecular diffusion. Since (in the present definitions) $D_\alpha > D_\beta$ we can expect ϕ_β to retain a longer memory as seen in the autocorrelations. This suggests that for $\tau > 0$ $\phi_\alpha(t)$ should be a better predictor of $\phi_\beta(t+\tau)$ than $\phi_\beta(t)$ is for $\phi_\alpha(t+\tau)$. In other words, the correlation between $\phi_\alpha(t)$ and

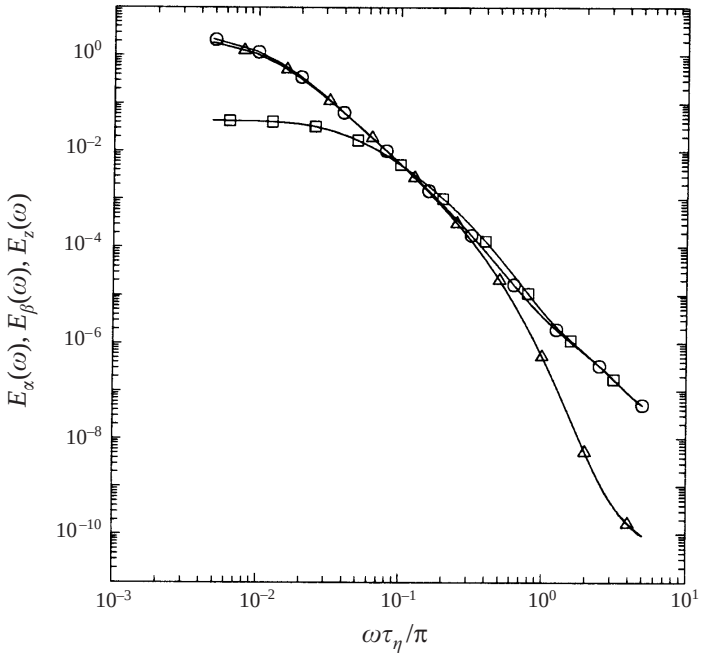

FIGURE 14. Lagrangian frequency spectra of two scalars at $Sc = 1/8$ (△), $Sc = 1$ (○) and their difference (□), from the 512^3 simulation. The data are shown as functions of the Kolmogorov-scaled frequency but the ordinate is unnormalized.

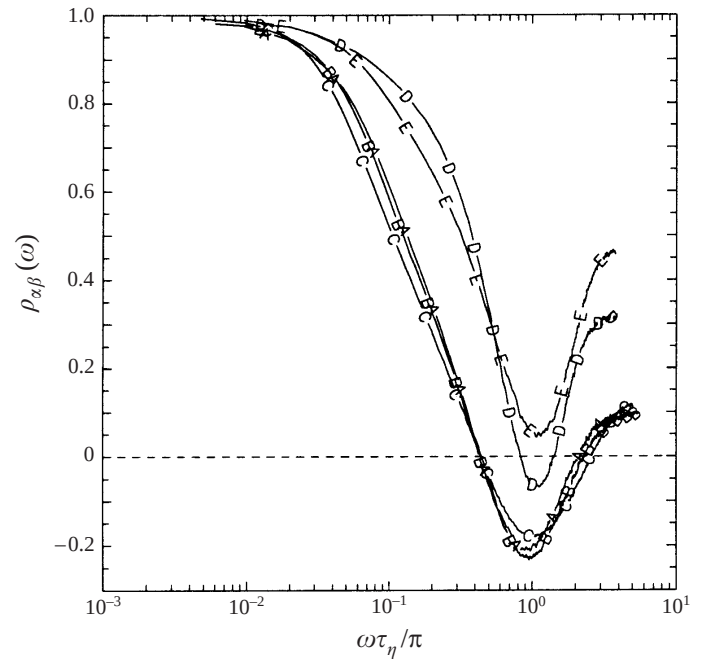

FIGURE 15. Lagrangian frequency spectrum of coherency between different scalars: $Sc = (1/8, 1)$ from the 128^3, 256^3 and 512^3 simulations (A,B,C) and $Sc = (1/4, 1)$ from the 64^3 and 128^3 (D,E). Data limitations at high frequencies are discussed in the text.

$\phi_\beta(t+\tau)$ is stronger than that between $\phi_\beta(t)$ and $\phi_\alpha(t+\tau)$, leading to (with the use of (25)) the observed asymmetry in figure 13.

Another important feature in figure 13 is that, consistent with the time series shown in figure 1(*c*, *d*, *e*), the difference autocorrelation is characterized by time scales shorter than those of both scalars in the pair. This is especially true at higher Reynolds numbers, where (as seen in figure 13*b*) the difference autocorrelation decays faster than the velocity autocorrelation.

Further information on time-scale ratios is given in table 6. The data for integral time scales reveal a slight dependence on Schmidt numbers, such that the ratio $\mathscr{T}_Z/T_L$ is somewhat larger for scalar pairs of more disparate Schmidt numbers (and hence stronger differential diffusion). On the other hand the Lagrangian Taylor time scale (τ_z) of z (defined in a manner similar to (22)) is about three times the Kolmogorov time scale, with no systematic dependence on either Reynolds or Schmidt numbers. Clearly, this suggests a degree of universality for the variation of z over small time intervals or at high frequencies.

In figure 14 we compare the frequency spectrum ($E_z(\omega)$) of z with those of each scalar taken separately, using data from the 512^3 simulation. It is clear that the spectra of ϕ_α and ϕ_β ($E_\alpha(\omega), E_\beta(\omega)$) differ mainly at higher frequencies, where the spectrum of z is seen to follow that of the less-diffusive scalar (ϕ_β) very closely. Although, as expected, all the spectra shown decrease monotonically with frequency, it appears that all curves ultimately begin to decay at a slower rate (from about $3\omega_\eta$ for ϕ_α and about $1.5\omega_\eta$ for ϕ_β and z). These reductions in decay rate are presumably due to numerical noise with origins as discussed at the end of § 4.2. The calculated spectra appear to be more robust at low frequencies, where $E_z(\omega)$ is seen to be low compared to both of $E_\alpha(\omega)$ and $E_\beta(\omega)$.

In a manner analogous to the coherency spectrum in Eulerian wavenumber space studied in Yeung (1996), it is of interest to examine the time-scale dependence of the correlation between different scalars in the Lagrangian frequency domain. In principle, considering 'in-phase' contributions only, the coherency spectrum can be defined as a spectral correlation coefficient, in terms of the spectra of each scalar and their co-spectrum (which is the proportional to the Fourier cosine transform of the cross-correlation function). However, as others reported in experiments (Mydlarski & Warhaft 1998), we find that the co-spectrum is subject to significantly higher noise levels, which can result in unphysical values of the coherency (outside the range $[-1, 1]$) at high frequencies. For our purposes better results are obtained by using the alternative relation

$$\rho_{\alpha\beta}(\omega) = \frac{[E_\alpha(\omega) + E_\beta(\omega) - E_z(\omega)]/2}{[E_\alpha(\omega)E_\beta(\omega)]^{1/2}}, \tag{26}$$

which is convenient because the autocorrelation of z is already computed and its frequency spectrum is readily obtained by a Fourier cosine transform.

Results on the coherency in Lagrangian frequency variables are given in figure 15 for scalar pairs at $Sc = (1/8, 1)$ for three different Reynolds numbers, and at $Sc = (1/4, 1)$ for two (lower) Reynolds numbers. At low frequencies the coherency is close to unity. At intermediate frequencies the coherency drops steadily, over a certain range where Kolmogorov scaling of the frequency produces a good 'collapse' of data at different Reynolds numbers. This observation is consistent with results in Yeung (1998) in which the similarity scaling behaviour of the Eulerian coherency spectrum in wavenumber space was investigated. The correlation coefficients between the Lagrangian time derivatives of the different scalars have also been computed

(see table 6), and are found to correspond to the coherency levels at intermediate frequencies.

At the high-frequency end of the data the coherency appears to attain a negative minimum and then rise again towards some non-trivial asymptotic value. This result has no clear physical basis, and is believed to be inaccurate. It may be noted that (see figure 14) at high frequencies it is very difficult to attain high accuracy in quantities appearing on the right-hand side of (26), and the observed anomalous behaviour may be a consequence of such uncertainties. It is also possible that numerical noise (perhaps arising from interpolation errors for fluid particle properties) becomes dominant at high frequencies, and that as in experiments (Mydlarski & Warhaft 1998) the noise contributions in different quantities may become spuriously correlated with each other.

5. Conclusions

In this work we have obtained and studied the Lagrangian time series of velocity and passive scalar fields via direct numerical simulations of isotropic turbulence, with grid resolution up to 512^3 and Taylor-scale Reynolds numbers between 38 and 234. Both velocity and scalar fields are stationary, under the respective influences of forcing at low wavenumbers and production by velocity fluctuations acting upon a uniform mean scalar gradient. Differential diffusion is studied in a Lagrangian frame for pairs of scalars with Schmidt numbers from 1/8 to 1. Data on all components of velocity and scalar gradients and hence the corresponding dissipation rates are also obtained. Information on Lagrangian scalar time series especially is new in the literature and important for the stochastic modelling of turbulent mixing. We discuss qualitative features of the raw time series (figures 1, 2, 4) as well as the behaviour of quantities from statistical processing, such as two-time correlation functions and frequency spectra.

In the case of statistics for the velocity field, the present high-resolution data allow an update of previous results (Yeung & Pope 1989) at lower Reynolds number. In particular we now find that, compared to the Lagrangian integral time scale (T_L, of the velocity), the integral time scales of both dissipation and (especially) enstrophy (vorticity squared) have a clear trend of decreasing with Reynolds number. The time series of both enstrophy and dissipation are characterized by short-lived intermittent bursts of intense activity. Relationships between the integral time scales of enstrophy and those of vorticity components are in part explained by a kinematic dimensionality effect. The Lagrangian frequency spectrum of the velocity is also calculated and found to suggest an emerging ω^{-2} range with a scaling constant which is consistent with previous estimates in the literature.

In the presence of a mean scalar gradient, it is important to note that the 'total' Lagrangian value ($\tilde{\phi}^+$) of each scalar carries contributions from both the instantaneous fluid particle position and the scalar fluctuation recorded along the particle trajectory. The variance of $\tilde{\phi}^+$ grows with time, at a rate determined by the velocity–scalar cross-correlation function (i.e. the correlation coefficient between $u^+(t)$ and $\phi^+(t+\tau)$) and the mean-square particle displacement (which dominates at large times). Cross-correlations are, in general, not symmetric functions of the time lag (τ); in this case the asymmetry (figure 7) can be traced to the fact that, due to advective transport, the velocity fluctuation at a given time t may have a strong effect on the scalar at a later time $t+\tau$ (with $\tau > 0$). Although not stationary, $\tilde{\phi}^+$ can be treated as a stochastic process with stationary increments, with the increments

($\Delta\tau\tilde{\phi}^+$) being of great interest in modelling, namely in the form of the mean of scalar diffusion conditioned upon fluctuations of both the velocity and the scalar. Despite considerable sampling noise a linear regression model for this quantity appears to agree well with the DNS data, with dependence on Reynolds and Schmidt numbers expressed via the model coefficients (table 3).

A comparison of autocorrelation functions (figure 10) shows that scalar fluctuations have longer Lagrangian time scales than the velocity, especially at higher Schmidt numbers where advective transport is more dominant than molecular diffusion. This behaviour is in contrast to the scalar dissipation, which becomes completely decorrelated more quickly than the energy dissipation, especially at higher Reynolds numbers but with little dependence on Schmidt number. The functional form of the scalar autocorrelation suggests a definite non-Markovian character, which may be important in devising suitable models. Comparisons are also made between Lagrangian and Eulerian rates of change for scalar fluctuations, including the scaling of Taylor time scales normalized by Kolmogorov variables. All results indicate a stronger role for advective transport (which constitutes the difference between these two rates of change) at higher Reynolds and/or Schmidt numbers. In addition, at intermediate frequencies there appears to be a limited ω^{-2} scaling range, followed by a wider $\omega^{-8/3}$ regime at higher Reynolds number.

To study the Lagrangian properties of differential diffusion we have calculated the two-scalar cross-correlation function ($\rho_{\alpha\beta}(\tau)$), as well as statistics of the difference z (i.e. $\phi_\alpha - \phi_\beta$) following fluid particles. The cross-correlation shows a definite skewness or asymmetry which is traced to the fact that the fluctuation of a less-diffusive scalar has a longer memory. The difference z is characterized by time scales much shorter (figures 1*e* and 13) than those of each scalar, including a Taylor time scale for its rate of change which is approximately three times the Kolmogorov time scale (table 6). This contrast in time scales is especially pronounced at higher Reynolds number, which is consistent with previous results (Yeung 1996, 1998) showing that the effects of differential diffusion remain important in the small scales. In addition the Lagrangian spectrum of z is found to follow that of the less-diffusive scalar at high frequencies. The difference spectrum is used to compute the coherency, which generally decreases with frequency but because of numerical noise is difficult to calculate accurately at frequencies higher than the Kolmogorov value.

In summary, we have performed a comprehensive study of Lagrangian time series in turbulence, including statistics of passive scalar transport which are new to the literature. Notable contrasts in time scales arise between Eulerian and Lagrangian rates of change (due to advective transport), and between scalar fluctuations of different Schmidt number and their difference (due to differential diffusion). The set of results we present spans a considerable Reynolds and Schmidt number range, made possible by high-resolution direct numerical simulations with up to 512^3 grid points. Together with additional quantities that can be computed from the database available, the current results are expected to be useful for the testing and further development of recent stochastic models of turbulent mixing. In addition, this work is to be extended to more general scenarios of multi-scalar mixing (e.g. Kronenburg & Bilger 1997).

The author gratefully acknowledges support from the National Science Foundation, via Grant CTS-9705678, and via NSF cooperative agreement ACI-9619020 through computing resources provided by the National Partnership for Advanced Computational Infrastructure at the San Diego Supercomputer Center. In addition

he thanks Rodney Fox, Laurent Mydlarski, Brian Sawford and Katepalli Sreenivasan for valuable discussions, as well as anonymous reviewers for helpful comments.

REFERENCES

Bilger, R. W. & Dibble, R. W. 1982 Differential molecular diffusion effects in turbulent mixing. *Combust. Sci. Tech.* **28**, 161–172.

Brethouwer, G. 2000 Mixing of passive and reactive scalars in turbulent flows: a numerical study. PhD dissertation, Delft University of Technology, the Netherlands.

Chen, S., Sreenivasan, K. R. & Nelkin, M. 1997 Inertial range scalings of dissipation and enstrophy in isotropic turbulence. *Phys. Rev. Lett.* **79**, 1253–1256.

Csanady, G. T. 1973 *Turbulent Diffusion in the Environment*. Reidel, Dordrecht.

Dopazo, C. 1994 Recent developments in PDF methods. In *Turbulent Reactive Flows* (ed. P. A. Libby & F. A. Williams), Academic.

Durbin, P. A. 1980 A stochastic model of two-particle dispersion and concentration fluctuations in homogeneous turbulence. *J. Fluid Mech.* **100**, 279–302.

Eswaran, V. & Pope, S. B. 1988*a* An examination of forcing in direct numerical simulations of turbulence. *Comput. Fluids* **16**, 257–278.

Eswaran, V. & Pope, S. B. 1988*b* Direct numerical simulations of the turbulent mixing of a passive scalar. *Phys. Fluids* **31**, 506–520.

Fox, R. O. 1995 The spectral relaxation model of the scalar dissipation in homogeneous turbulence. *Phys. Fluids* **7**, 1082–1094.

Fox, R. O. 1996 On velocity-conditioned scalar mixing in homogeneous turbulence. *Phys. Fluids* **8**, 2678–2691.

Fox, R. O. 1997 The Lagrangian spectral relaxation model of the scalar dissipation in homogeneous turbulence. *Phys. Fluids* **9**, 2364–2386.

Fox, R. O. 1999 The Lagrangian spectral relaxation model for differential diffusion in homogeneous turbulence. *Phys. Fluids* **11**, 1550–1571.

Frisch, U. 1995 *Turbulence*. Cambridge University Press.

Fung, J. C. H. & Vassilicos, J. C. 1998 Two-particle dispersion in turbulentlike flows. *Phys. Rev.* E **57**, 1677–1690.

Gotoh, T. & Rogallo, R. S. 1999 Intermittency and scaling of pressure at small scales in isotropic forced turbulence. *J. Fluid Mech.* **396**, 257–285.

Heppe, B. M. O. 1997 Generalized Langevin equation and relative turbulent dispersion. *J. Fluid Mech.* **357**, 167–198.

Kimura, Y. & Herring, J. R. 1996 Diffusion in stably stratified turbulence. *J. Fluid Mech.* **328**, 253–269.

Klimenko, A. Y. & Bilger, R. W. 1999 Conditional moment closure for turbulent combustion. *Progr. Energy Combust. Sci.* **25**, 595–687.

Kronenburg, A. & Bilger, R. W. 1997 Modelling of differential diffusion effects in nonpremixed nonreacting turbulent flow. *Phys. Fluids* **9**, 1435–1447.

Malik, N. A. & Vassilicos, J. C. 1999 A Lagrangian model for turbulent dispersion with turbulent-like flow structure: comparison with direct numerical simulation for two-particle statistics. *Phys. Fluids* **11**, 1572–1580.

Monin, A. S. & Yaglom, A. M. 1971 *Statistical Fluid Mechanics*, Vol. I (ed. J. L. Lumley). MIT Press.

Monin, A. S. & Yaglom, A. M. 1975 *Statistical Fluid Mechanics*, Vol. II (ed. J. L. Lumley). MIT Press.

Mydlarski, L. & Warhaft. Z. 1998 Passive scalar statistics in high-Péclet-number grid turbulence. *J. Fluid Mech.* **358**, 135–175.

Nilsen, V. & Kosály, G. 1997 Differentially diffusing scalars in turbulence. *Phys. Fluids* **9**, 3386–3397.

Ooi, A., Martin, J., Soria, J. & Chong, M. S. 1999 A study of the evolution and characteristics of the invariants of the velocity-gradient tensor in isotropic turbulence. *J. Fluid Mech.* **381**, 141–174.

Overholt, M. R. & Pope, S. B. 1996 Direct numerical simulation of a passive scalar with imposed mean gradient in isotropic turbulence. *Phys. Fluids* **8**, 3128–3148.

Pope, S. B. 1985 PDF methods for turbulent reactive flows. *Progr. Energy Combust. Sci.* **11**, 119–192.

Pope, S. B. 1994 Lagrangian pdf methods for turbulent flows. *Ann. Rev. Fluid Mech.* **26**, 23–63.

Pope, S. B. 1998 The vanishing effect of molecular diffusivity on turbulent dispersion: implications for turbulent mixing and the scalar flux. *J. Fluid Mech.* **359**, 299–312.

Pope, S. B. 2000 *Turbulent Flows*. Cambridge University Press.

Priestley, M. B. 1981 *Spectral Analysis and Time Series*. Academic.

Riley, J. J. & Patterson, G. S. 1974 Diffusion experiments with numerically integrated isotropic turbulence. *Phys. Fluids* **17**, 292–297.

Rogallo, R. S. 1981 Numerical experiments in homogeneous turbulence. *NASA Tech. Memo*. 81315. NASA Ames Research Center.

Sawford, B. L. 1985 Lagrangian statistical simulation of concentration mean and fluctuation fields. *J. Clim. Appl. Met.* **24**, 1152–1166.

Sawford, B. L. 1991 Reynolds number effects in Lagrangian stochastic models of turbulent dispersion. *Phys. Fluids* A **3**, 1577–1586.

Saylor, J. R. & Sreenivasan, K. R. 1998 Differential diffusion in low Reynolds number water jets. *Phys. Fluids* **10**, 1135–1146.

Squires, K. D. & Eaton, J. K. 1991 Lagrangian and Eulerian statistics obtained from direct numerical simulations of homogeneous turbulence. *Phys. Fluids* A **3**, 130–143.

Sreenivasan, K. R. 1991 On the local isotropy of passive scalars in turbulent shear flows. In *Turbulence and Stochastic Processes: Kolmogorov's Ideas 50 Years On* (ed. J. C. R. Hunt, O. M. Phillips & D. Williams), pp. 165–182. Royal Society, London.

Sreenivasan, K. R. 1995 On the universality of the Kolmogorov constant. *Phys. Fluids* **7**, 2778–2784.

Sreenivasan, K. R. 1996 The passive scalar spectrum and the Obukhov-Corrsin constant. *Phys. Fluids* **8**, 189–196.

Sreenivasan, K. R. & Antonia, R. A. 1997 The phenomenology of small-scale turbulence. *Ann. Rev. Fluid Mech.* **29**, 435–472.

Swaminathan, N. & Bilger, R. W. 1999 Study of the conditional covariance and variance equations for second order CMC. *Phys. Fluids* **11**, 2679–2695.

Taylor, G. I. 1921 Diffusion by continuous movements. *Proc. Lond. Math. Soc.* (2) **20**, 196–211.

Tennekes, H. 1975 Eulerian and Lagrangian time microscales in isotropic turbulence. *J. Fluid Mech.* **67**, 561–567.

Tennekes, H. & Lumley, J. L. 1972 *A First Course in Turbulence*. MIT Press.

Thomson, D. J. 1996 The second-order moment structure of dispersing plumes and puffs. *J. Fluid Mech.* **320**, 305–329.

Tsai, K. & Fox, R. O. 1995 Modeling multiple reactive scalar mixing with the generalized IEM model. *Phys. Fluids* **7**, 2820–2830.

Ulitsky, M. & Collins, L. R. 2000 On constructing realizable conservative mixed-scalar equations using the eddy damped quasi-normal Markovian theory. *J. Fluid Mech.* **412**, 303–329.

Valiño, L. & Dopazo, C. 1990 A binomial sampling model for scalar turbulent mixing. *Phys. Fluids* A **2**, 1204–1212.

Valiño, L. & Dopazo, C. 1991 A binomial Langevin model for turbulent mixing. *Phys. Fluids* A **3**, 3034–3037.

Vedula, P. & Yeung, P. K. 1999 Similarity scaling of acceleration and pressure statistics in numerical simulations of isotropic turbulence. *Phys. Fluids* **11**, 1208–1220.

Voth, G. A., Satyanarayanan, K. & Bodenschatz, E. 1998 Lagrangian acceleration measurements at large Reynolds numbers. *Phys. Fluids* **10**, 2268–2280.

Warhaft, Z. 2000 Passive scalars in turbulent flows. *Ann. Rev. Fluid Mech.* **32**, 203–240.

Yeung, P. K. 1996 Multi-scalar spectral transfer in differential diffusion with and without mean scalar gradients. *J. Fluid Mech.* **321**, 235–278.

Yeung, P. K. 1997 One- and two-particle Lagrangian acceleration correlations in numerically simulated homogeneous turbulence. *Phys. Fluids* **9**, 2981–2990.

Yeung, P. K. 1998 Correlations and conditional statistics in differential diffusion: scalars with mean scalar gradients. *Phys. Fluids* **10**, 2621–2635.

Yeung, P. K. & Fox, R. O. 1999 Lagrangian statistics of passive scalars in isotropic turbulence: A

comparison of simulation and modeling. Presented at 1999 Annual Meeting, American Society of Chemical Engineers, Dallas, TX, Oct–Nov. 1999.

YEUNG, P. K. & POPE, S. B. 1988 An algorithm for tracking fluid particles in numerical simulations of homogeneous turbulence. *J. Comput. Phys.* **79**, 373–416.

YEUNG, P. K. & POPE, S. B. 1989 Lagrangian statistics from direct numerical simulations of isotropic turbulence. *J. Fluid Mech.* **207**, 531–586.

YEUNG, P. K. & ZHOU, Y. 1997 On the universality of the Kolmogorov constant in numerical simulations of turbulence. *Phys. Rev.* E **56**, 1746–1752.